Geostrophic Closure of the Zonally Averaged Atlantic Meridional Overturning Circulation

FLORIAN SÉVELLEC

Ocean and Earth Science, National Oceanography Centre Southampton, University of Southampton, Southampton, United Kingdom

THIERRY HUCK

Laboratoire de Physique des Océans (UMR 6523 CNRS IFREMER IRD UBO), Brest, France

(Manuscript received 24 July 2014, in final form 29 May 2015)

ABSTRACT

It is typically assumed that the meridional density gradient in the North Atlantic is well and positively correlated with the Atlantic meridional overturning circulation (AMOC). In numerical "water-hosing" experiments, for example, imposing an anomalous freshwater flux in the Northern Hemisphere leads to a slowdown of the AMOC. However, on planetary scale, the first-order dynamics are linked to the geostrophic balance, relating the north–south pressure gradient to the zonal circulation. In this study, these two approaches are reconciled. At steady state and under geostrophic dynamics, an analytical expression is derived to relate the zonal and meridional pressure gradient. This solution is only valid where the meridional density gradient length scale is shorter than Earth's curvature length scale, that is, north of 35°N. This theoretical expression links the north–south density gradient to the AMOC and can be used as a closure for zonally averaged ocean models. Assumptions and shortcomings of the approach are presented. Implications of these results for paleoclimate problems such as AMOC collapse and asymmetry in the meridional overturning circulation of the Atlantic and of the Pacific are discussed.

1. Introduction

The ocean carries roughly 1.3 PW northward in the North Atlantic (Ganachaud and Wunsch 2000; Lumpkin and Speer 2007). This heat transport is primarily achieved by the Atlantic meridional overturning circulation (AMOC). This baroclinic circulation can be schematically described by a northward surface flow of relative warm water and a cold southward return flow at depth (Sévellec and Fedorov 2011). The warm surface branch exchanges heat with the atmosphere, warming northern regions of the North Atlantic (Gagosian 2003). This process contributes to the climate of these regions and partially explains the mild European climate. It has been conjectured, through the use of a coupled general circulation model (GCM), that a shutdown of the AMOC could cool down Europe by 1–3 K (Vellinga and Wood 2002; Stouffer et al. 2006).

The AMOC intensity has been shown to be accurately measured through the eastern–western density difference (Hirschi et al. 2003; Rayner et al. 2011) and has been monitored using this property since early 2006 at 26°N (McCarthy et al. 2012). This measurement takes advantage of the geostrophic thermal wind balance, relating the zonal gradient of baroclinic pressure to the baroclinic meridional flow (Vallis 2006). In parallel to the observational studies, "hosing experiments" have shown that the AMOC is sensitive to the meridional density gradient (Rahmstorf 1995; Manabe and Stouffer 1995, 1999; Rind et al. 2001; Stouffer et al. 2006; Barreiro et al. 2008 and references therein). These experiments consist of an exogenous freshening of the northern North Atlantic and show a reduction or a collapse of the AMOC in numerical simulations with state-of-the-art

Denotes Open Access content.

Corresponding author address: Florian Sévellec, Ocean and Earth Sciences, University of Southampton, Waterfront Campus, European Way, Southampton SO14 3ZH, United Kingdom.
E-mail: florian.sevellec@noc.soton.ac.uk

DOI: 10.1175/JPO-D-14-0148.1

ocean models (Stouffer et al. 2006). In this context, de Boer et al. (2010) link the AMOC intensity to the meridional pressure gradient (rather than the density gradient) in a set of coupled numerical experiments. Despite being at the base of the scaling of the AMOC and its heat transport as a function of diapycnal eddy diffusivity, for instance (Park and Bryan 2000, and references therein), or being at the base of recent theoretical description of the AMOC (Nikurashin and Vallis 2012), this empirical relation between the meridional density or pressure gradient and the AMOC has not yet been properly established.

Attempts to rationalize this relation have always been constrained by some degrees of parameterization (Marotzke et al. 1988; Wright and Stocker 1991; Wright et al. 1995; Drbohlav and Jin 1998; Olbers et al. 2012). Despite this shortcoming, this relation has been widely used to develop zonally averaged ocean models. These models have been shown to accurately represent the ocean dynamics in term of water mass properties as well as heat and freshwater transports (Knutti et al. 2000; Sévellec and Fedorov 2011). Although 3D ocean GCMs are fully available to the climate community, the use of the intermediate complexity model is still of significant importance. For example, in the context of paleoclimate studies, the use of zonally averaged ocean models is particularly beneficial since it considerably reduces the numerical cost and allows for long time integrations (Stocker et al. 1992, for instance).

To overcome the difficulty of writing a zonally averaged ocean model as a closed self-consistent problem, Marotzke et al. (1988) suggest exclusively using an enhanced friction term (a vertical Laplacian) to balance the pressure gradient in the meridional momentum equation. In Wright and Stocker (1991), the authors assumed a relation between the zonal and meridional pressure gradients. Using this assumption, the meridional momentum equation could be rewritten and virtually corresponds to an enhanced Rayleigh friction balancing the pressure gradient. In that study, Wright and Stocker (1991) show that such linear relation between the meridional and zonal pressure gradients holds well in an ocean GCM. Drbohlav and Jin (1998) suggested using the parameterization of Wright and Stocker (1991) together with keeping the acceleration and inertial terms in the meridional momentum equation. This incorporates meridional velocity adjustment and higher-frequency variability, partially solving (maybe incorrectly) the lack of decadal variability of zonally averaged model. This method is highly speculative since the closure of Wright and Stocker (1991) implicitly assumed a baroclinic zonal adjustment (baroclinic Rossby waves acting on a decadal time scale). Wright et al. (1998) provided an explanation for the parameterization based on geometric arguments between a western boundary layer and a geostrophic interior flow. Nevertheless, the solution required the parameterization of several terms. Wright et al. (1995) suggested a new closure scheme based on vorticity dissipation along the western boundary. This method, including nonlocal effects, largely increases the accuracy of the zonally averaged ocean model. However, this closure scheme is still dependent on parameters that are chosen to make the ocean circulation as accurate as possible. Olbers et al. (2012) revised some limitations of Wright et al. (1995). More recently, Sijp et al. (2012) demonstrate, without any parameterization, a relation between the meridional flow and the meridional pressure gradient at low latitude (i.e., equatorial region), where the β-plane approximation can be used. To obtain such a result, the authors assumed weak zonal flow. This is debatable in the equatorial context, where the Atlantic Equatorial Undercurrent can reach $1\,\mathrm{m\,s^{-1}}$ in 10 days average (compared to the $0.2\,\mathrm{m\,s^{-1}}$ meridional current; Giarolla et al. 2005). In this framework, the authors show that potential energy arising from the meridional slope of isopycnals is converted into kinetic energy, sustaining the AMOC, and then viscously dissipated.

Here, we will follow the same analytical methodology to overcome the need of parameterization in the zonally averaged ocean model, but we will not specifically concentrate on the equatorial dynamics. As suggested by Colin de Verdière and Tailleux (2005), the ocean dynamics have two regimes depending on the role of the vertical advection versus the horizontal advection in the tracer(s) evolution. If the former dominates, the regime is more inclined to free propagation of a Rossby wave. At the opposite, if horizontal advection dominates, the regime acts almost like on an f plane. These two regimes correspond to the southern and northern parts of the North Atlantic, respectively. From an observational perspective, in the former region the AMOC is strongly controlled by the boundary current (e.g., the Florida Current at 26°N; McCarthy et al. 2012), whereas in the latter region the AMOC is an interior process through the North Atlantic Drift.

In the context of the latter regime, we will demonstrate that, under some assumptions, the zonal and meridional geostrophic flows are related. This relation suggests the validity of ocean zonally averaged models. An advantage of this analytical method is that it also determines the range of validity of this relation because we know and we can test the assumptions made to obtain it. We show that this relation is valid in the north of the North Atlantic and because the basin is bounded zonally (vs periodical as in the Southern Ocean). We anticipate that in the southern part of the North Atlantic the

boundary consideration of Wright et al. (1998) is probably more accurate.

The goal of our study is not to develop a theory or a full solution of the AMOC but rather to demonstrate the existence of a closure for the zonally averaged problem, valid in a limited region. There exists theory of the AMOC (e.g., Gnanadesikan 1999; Wolfe and Cessi 2011; Nikurashin and Vallis 2012) or numerical investigation of the full nonlinear problem (e.g., Sévellec and Fedorov 2011). However, all these studies assume explicitly or implicitly a relation between the meridional density gradient and the meridional flow. Thus, determining the existence and the limit of zonally averaged closure for the AMOC remains a timely effort.

Therefore, we will have two main objectives: 1) We will analytically demonstrate the dependency of the AMOC intensity to the meridional density gradient and thus explain on a theoretical ground the AMOC shutdown to a freshwater release in the north of the North Atlantic. 2) We will suggest a zonally averaged model of the AMOC forced by the wind and stratification, inspired by the work of Stommel (1948) and Munk (1950) in the context of the wind-forced barotropic circulation.

These two objectives are reached starting from planetary-geostrophic equations with Rayleigh-type linear friction, considering a known stratification (function of both temperature and salinity) and wind stresses. We have tested two different cases of surface boundary layer: an implicit boundary layer where the Ekman pumping is imposed at the ocean surface and an explicit boundary layer resolving the surface dynamics using a Laplacian vertical viscosity in the horizontal momentum equations.

We show that a zonally averaged solution can be derived under two main assumptions: 1) The meridional density gradient length scale is shorter than Earth's curvature length scale, limiting our result to regions of high isopycnal slope, that is, north of 35°N. This assumption is similar to the equivalent-barotropic circulation of Killworth and Hughes (2002) that holds well in the northern part of the North Atlantic. 2) The zonal density gradient is zonally uniform (i.e., the meridional geostrophic velocities are zonally uniform). These needed assumptions give the limit of validity of our zonally averaged ocean model. In this context, the solution corresponds to a thermohaline circulation pushing the system toward a minimum of available potential energy.

The structure of the paper is as follows: In section 2, the set of equations, the configuration, and the synthetic forcing of the model is described. In section 3, we apply the zonal averaging. We also demonstrate, under some assumptions, the geostrophic zonally averaged closure, that is, the relation between meridional and zonal density gradients. The general solution of the AMOC and the application to the synthetic forcing are given in section 4. Discussion is given in section 5, and conclusions and directions for future work are described in section 6.

TABLE 1. Parameter values of the model.

Parameter	Value	Description
y_0	10°N	Southern basin boundary
y_1	70°N	Northern basin boundary
H	4500 m	Ocean depth
W	4000 km	Zonal basin extent
g	$9.8\,\mathrm{m\,s^{-2}}$	Acceleration of gravity
ρ_0	$1027\,\mathrm{kg\,m^{-3}}$	Reference density
α_T	$2.2\times10^{-4}\,\mathrm{K^{-1}}$	Thermal expansion coefficient
α_S	$7.7\times10^{-4}\,\mathrm{psu^{-1}}$	Haline contraction coefficient
R_E	$6.4\times10^{6}\,\mathrm{m}$	Earth's radius
C_p	$4.0\times10^{3}\,\mathrm{J\,kg^{-1}\,K^{-1}}$	Specific heat for seawater
T_0	2°C	Reference temperature
ΔT	24°C	Temperature difference
S_0	35 psu	Reference salinity
ΔS	0.6 psu	Salinity difference
h	1000 m	Pycnocline depth
τ_x^0	$0.1\,\mathrm{N\,m^{-2}}$	Zonal wind stress intensity
τ_y^0	$0.05\,\mathrm{N\,m^{-2}}$	Meridional wind stress intensity
λ	$10^{-6}\,\mathrm{s^{-1}}$	Linear friction coefficient
ν	$10^{-4}\,\mathrm{m^2\,s^{-1}}$	Vertical viscosity coefficient

2. The set of equations, model configuration, and synthetic forcing

a. Model configuration

The theoretical model configuration consists of a flat-bottom rectangular basin representing the North Atlantic (from $y_0 = 10$°N to $y_1 = 70$°N). The depth of the ocean is $H = 4500$ m, and its zonal extent is $W = 4000$ km (Table 1). The rotation rate varies according to the curvature of Earth (Fig. 1). We suppose the ocean stratification is known and depends on both zonally averaged temperature and salinity fields. The momentum is forced at the surface by wind stresses.

b. Model equations

We start from the 3D set of equations typical of the planetary-geostrophic regime [geostrophic regime of type 2 in Phillips (1963), Colin de Verdière (1988), and Salmon (1998)]: the geostrophic balance together with a Rayleigh friction, the hydrostatic, the nondivergence, and the time evolution of density. This corresponds to a low Rossby number (Ro $\ll 1$, measuring the ratio of inertial terms to Coriolis terms in the horizontal momentum equations). In Cartesian geometry, this set of equations can be mathematically written as

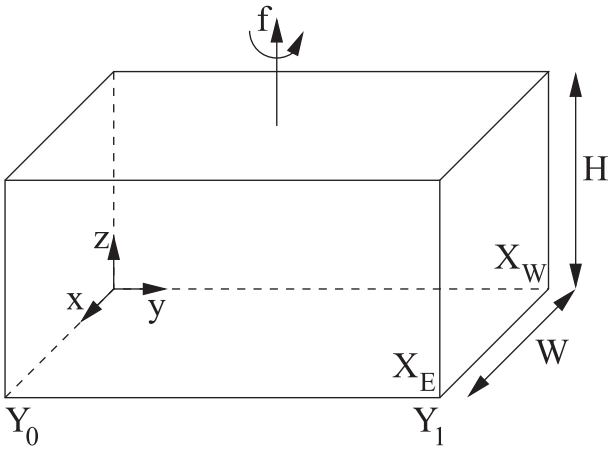

FIG. 1. Configuration of the idealized basin. The variables x, y, and z are the zonal, meridional, and vertical coordinates; W is the zonal width, H is the depth, f is the local Coriolis parameter, y_0 and y_1 are the latitudes of the southern and northern boundaries, and x_E and x_W are the longitudes of the eastern and western boundaries.

$$-fv = -\frac{1}{\rho_0}\partial_x P - \lambda u, \tag{1a}$$

$$fu = -\frac{1}{\rho_0}\partial_y P - \lambda v, \tag{1b}$$

$$\partial_z P = -\rho g, \tag{1c}$$

$$\partial_x u + \partial_y v + \partial_z w = 0, \quad \text{and} \tag{1d}$$

$$D_t \rho = \text{Diff}, \tag{1e}$$

where t is the time; x, y, and z are the zonal, meridional, and vertical coordinates; ρ_0 is the reference density; f is the Coriolis parameter; λ is the Rayleigh friction coefficient; u, v, and w are the zonal, meridional, and vertical velocities; T is the temperature; S is the salinity; P is the pressure; ρ is the density as a function of T, S, and P through the equation of state of seawater; D_t is the material derivative ($=\partial_t + u\partial_x + v\partial_y + w\partial_z$); and Diff is the eddy diffusivity operator for density. Parameter values are given in Table 1.

For this set of equations to be well posed, a friction term should be retained in the vertical momentum balance: $\partial_z P = -\rho g - \rho_0 \lambda_v w$, where λ_v is the vertical friction coefficient (Salmon 1998). This term is fundamental to allow boundary conditions such as no heat flux ($\partial_n \rho = 0$, where n is the coordinate of the direction normal to the local boundary) together with a rigid boundary ($u_n = 0$, where u_n is the velocity normal to the local boundary) without setting pressure at the boundary to a constant (which inherently filters out zonally averaged meridional geostrophic flow). This means that, at the boundary, the vertical velocity would be important to balance the pressure gradient: $\partial_n w|_{n=0} = \partial_z \partial_n P|_{n=0}/(\lambda_v \rho_0)$. However, on the first order, and since we will not prescribe heat transfer at the horizontal boundaries, one could neglect this friction term and apply the hydrostatic relation $\partial_z P = -\rho g$. For more extensive discussion and numerical investigations, we refer the reader to appendix A and to the study of Huck et al. (1999).

c. Synthetic forcing

The zonal and meridional wind stresses over the North Atlantic are represented by sinusoidal functions of the meridional position only:

$$\tau_x = -\tau_x^0 \sin\left(2\pi \frac{y - y_0}{y_1 - y_0}\right), \quad \text{and} \tag{2a}$$

$$\tau_y = -\tau_y^0 \sin\left(2\pi \frac{y - y_0}{y_1 - y_0}\right), \tag{2b}$$

where τ_x and τ_y are the zonal and meridional wind stresses, respectively, and τ_x^0 and τ_y^0 are their respective intensity.

The stratification is composed of temperature and salinity fields. The temperature and salinity follow a simple cosine and sine dependence on latitude, respectively. On the vertical we apply an exponential decay. Their mathematical expressions are

$$T = T_0 + \Delta T \cos\left(\frac{\pi}{2} \frac{y - y_0}{y_1 - y_0}\right) e^{z/h}, \quad \text{and} \tag{3a}$$

$$S = S_0 + \Delta S \sin\left(\pi \frac{y - y_0}{y_1 - y_0}\right) e^{z/h}, \tag{3b}$$

where T_0 and S_0 are reference temperature and salinity, respectively, and ΔT and ΔS are temperature and salinity difference, respectively. The scalar h is the typical vertical scale of the pycnocline. Parameter values are given in Table 1.

Overall, the temperature and salinity fields, as well as the zonal and meridional wind stresses, correspond to a realistic forcing of our set of equations (Fig. 2). Temperature and salinity are converted into density using a linear equation of state of seawater:

$$\rho = \rho_0[1 - \alpha_T(T - T_0) + \alpha_S(S - S_0)], \tag{4}$$

where α_T and α_S are the thermal expansion and haline contraction coefficients, respectively.

3. Zonal averaging and closure

a. Zonal averaging of the tracer evolution equation

Rewriting the evolution of tracer from (1) and using the Laplacian operator for tracer diffusion, we can

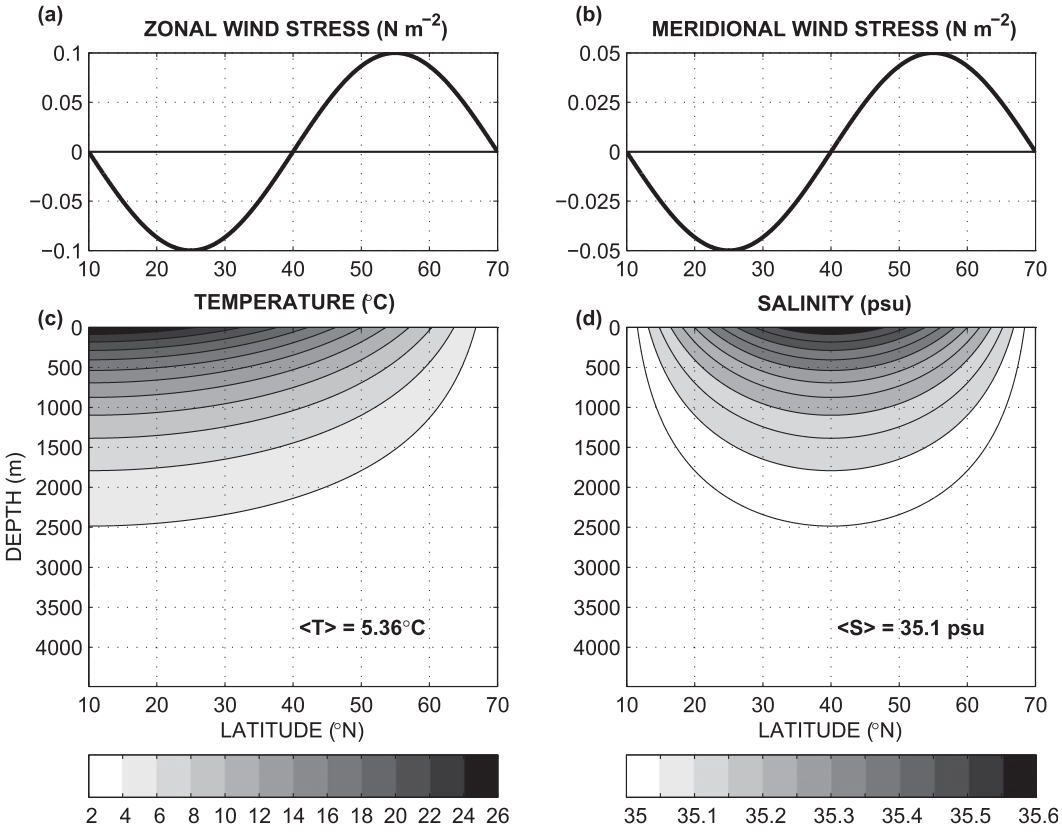

FIG. 2. Analytical forcing terms of the set of equations: (a) zonal and (b) meridional wind stress and zonally averaged (c) temperature and (d) salinity. Contour intervals for temperature and salinity are 2 K and 0.05 psu, respectively.

express the evolution of any tracer θ (e.g., density, temperature, or salinity) as

$$\partial_t\theta = -u\partial_x\theta - v\partial_y\theta - w\partial_z\theta + \partial_x(k_x\partial_x\theta) + \partial_y(k_y\partial_y\theta) + \partial_z(k_z\partial_z\theta), \quad (5)$$

where k_x, k_y, and k_z are the zonal, meridional, and vertical eddy diffusion coefficients, respectively.

This expression is zonally averaged using a solid adiabatic boundary condition in the east and west of the basin: $u|_{x_W} = u|_{x_E} = 0$ and $\partial_x\theta|_{x_W} = \partial_x\theta|_{x_E} = 0$, where x_W and x_E are the western and eastern zonal boundary limits of the basin, respectively. We define the zonal average $\overline{X}$ of any variable X as $\overline{X} = W^{-1}\int_{x_W}^{x_E} X\,dx$, where W is the zonal width of the basin $(x_E - x_W)$ and dx is the zonal unit coordinate. Assuming the uniformity of the meridional and vertical diffusion coefficients in the zonal direction ($\partial_x k_y = 0$ and $\partial_x k_z = 0$), we obtain

$$\partial_t\overline{\theta} = -\partial_y\overline{v\theta} - \partial_z\overline{w\theta} + \partial_y(k_y\partial_y\overline{\theta}) + \partial_z(k_z\partial_z\overline{\theta}). \quad (6)$$

Using the same solid boundary conditions ($u|_{x_W} = u|_{x_E} = 0$), the nondivergence (1d) can also be zonally averaged:

$$\partial_y\overline{v} + \partial_z\overline{w} = 0. \quad (7)$$

From these expressions, one can see that the advection terms are the difficult part to estimate, because they are not only dependent on the zonally averaged dynamics but also on the cross correlation of the zonal anomaly of tracer and velocities. To overcome this issue, we define equivalent meridional and vertical velocities as $\tilde{v}_\theta = \overline{v\theta}/\overline{\theta}$ and $\tilde{w}_\theta = \overline{w\theta}/\overline{\theta}$. In the context of the temperature and salinity (the two tracers that affect the density and hence the velocity), we diagnose these equivalent velocities in an ocean GCM (NEMO–OPA in its ORCA2 configuration; Madec et al. 1998). These diagnostics suggest $\tilde{v}_{T/S} \simeq \overline{v}$ and $\tilde{w}_{T/S} \simeq \overline{w}$. We find that the error is below ±15% for temperature and is negligible for salinity (Fig. 3).

We can thus write on first order that

$$\partial_t\overline{\theta} \simeq -\overline{v}\partial_y\overline{\theta} - \overline{w}\partial_z\overline{\theta} + \partial_y(k_y\partial_y\overline{\theta}) + \partial_z(k_z\partial_z\overline{\theta}), \quad (8)$$

where θ is either temperature or salinity. By using this last expression, one assumes that, at leading order, the dynamics is equivalent to a zonally averaged dynamics; that is, the heat and freshwater transport is primarily

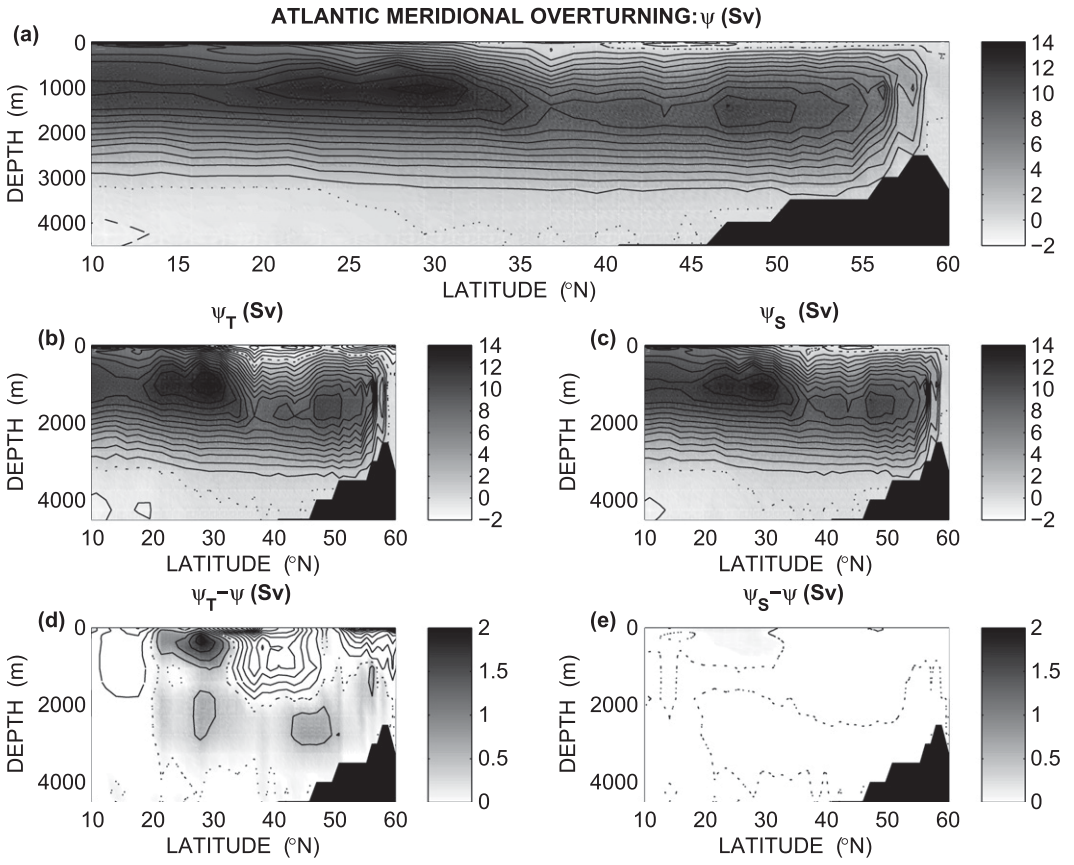

FIG. 3. (a) Overturning streamfunction, defined as $\partial_z\psi = -W\overline{v}$ and $\partial_y\psi = W\overline{w}$, in an ocean GCM (NEMO-OPA in its ORCA2 configuration; Madec et al. 1998). (b),(c) Overturning streamfunctions defined using equivalent velocities ($\tilde{v}_\theta = \overline{v\theta}/\overline{\theta}$ and $\tilde{w}_\theta = \overline{w\theta}/\overline{\theta}$) for both dynamical tracers: temperature and salinity. (d) Differences between (b) and (a) and (e) differences between (c) and (a). (a)–(c) Solid, dashed, and dotted lines represent positive, negative and zero values, respectively. (d)–(e) Grayscale shading is superimposed to the contours for positive values (following the white-to-black color bar scale), and negative values are shown by contours without the white-to-black shading superimposed. Contour interval is 1 Sv for (a)–(c) and 0.5 Sv for (d)–(e). Positive values denote clockwise circulation.

done by the overturning circulation rather than the horizontal circulation. Since the horizontal circulation is more intense than the overturning one in terms of mass transport, the accuracy of this assumption derives from the stronger vertical gradient compared to the zonal one for both temperature and salinity.

b. *Zonal averaging of momentum equations*

To derive the rest of the zonally averaged ocean model, we restart with the momentum equations from (1). We introduce the hydrostatic relation into the vertically differentiated horizontal momentum equations, leading to the thermal wind relation with friction:

$$-f\partial_z v = \frac{g}{\rho_0}\partial_x \rho - \lambda \partial_z u, \quad \text{and} \tag{9a}$$

$$f\partial_z u = \frac{g}{\rho_0}\partial_y \rho - \lambda \partial_z v. \tag{9b}$$

Rearranging these equations to separate the contribution of the zonal and meridional velocities, and after zonal averaging, we obtain:

$$(f^2+\lambda^2)\partial_z \overline{u} = \frac{g}{\rho_0}\left(\lambda \frac{\rho|_{x_E} - \rho|_{x_W}}{W} + f\partial_y \overline{\rho}\right), \quad \text{and} \tag{10a}$$

$$(f^2+\lambda^2)\partial_z \overline{v} = \frac{g}{\rho_0}\left(\lambda \partial_y \overline{\rho} - f\frac{\rho|_{x_E} - \rho|_{x_W}}{W}\right), \tag{10b}$$

where $\rho|_{x_E}$ and $\rho|_{x_W}$ are the density values at the eastern and western basin boundaries, respectively.

Since friction is small ($\lambda \ll f$), these relations relate the vertical shear of meridional and zonal velocities to the zonal and meridional density gradient, respectively. Especially the zonally averaged meridional velocities are related to the density difference between the eastern and western edges of the basin. This last relation is

equivalent to what is operationally used to compute the AMOC intensity from the RAPID array (Hirschi and Marotzke 2007). However, this relation is not useful to consistently represent the circulation in a 2D depth-latitude plan since it links the meridional flow to the eastern–western density difference. For that purpose, following the idea of Wright and Stocker (1991), one needs to relate the geostrophic eastern–western density difference to the geostrophic meridional density gradient.

c. *Closure through horizontal geostrophic transports balance*

We restart from (1), but limit our study to a high Reynolds number (Re $\gg 1$, i.e., the ratio of advection to dissipation in horizontal momentum equations). This corresponds to an interior solution, away from the vicinity of viscous horizontal and vertical boundary layers. Under this assumption, we obtain the geostrophic balance:

$$f v_g = \frac{1}{\rho_0}\partial_x P, \quad \text{and} \tag{11a}$$

$$f u_g = -\frac{1}{\rho_0}\partial_y P, \tag{11b}$$

where u_g and v_g are the zonal and meridional geostrophic velocities, respectively. The Sverdrup balance (Sverdrup 1947) is obtained by introducing the geostrophic balance in the nondivergence [(1d)]:

$$\beta v_g = f\partial_z w, \tag{12}$$

where $\beta = \partial_y f$ is the meridional variation of the Coriolis parameter.

The thermal wind relation is obtained by applying the hydrostatic equation to (11):

$$-f\partial_z v_g = \frac{g}{\rho_0}\partial_x \rho, \quad \text{and} \tag{13a}$$

$$f\partial_z u_g = \frac{g}{\rho_0}\partial_y \rho. \tag{13b}$$

The density evolution [(1e)] with a high Péclet number (Pe $\gg 1$, i.e., the ratio of advection to diffusion in the density evolution) reads $\partial_t\rho + u\partial_x\rho + v\partial_y\rho + w\partial_z\rho = 0$. Thus, applying the last relations, (12) and (13), to this density evolution leads to

$$\partial_t \rho = \frac{f^2\rho_0}{\beta g}(u_g\partial_z^2 w - \partial_z u_g \partial_z w) - w\partial_z\rho. \tag{14}$$

This relation suggests that, at steady state ($\partial_t \to 0$), the vertical flow, and thus the meridional one through (12), is only a function of meridional pressure and density gradients and stratification. This is a glimpse that the geostrophic flow could be perfectly known in a latitude-depth framework.

At steady state, a scaling analysis suggests two results: (i) the zonal and meridional advection are comparable, $|u\partial_x\rho|/|v\partial_y\rho| \simeq |u_g\partial_z^2 w|/|\partial_z u_g \partial_z w| \sim 1$, and (ii) the ratio of vertical advection to meridional advection, $|w\partial_z\rho|/|v\partial_y\rho| \simeq |w\partial_z\rho|/|(f/\beta)\partial_y\rho\partial_z w|$, scales as $\epsilon = l\beta/f$ (where l is the meridional extent of the pycnocline $l = -h\partial_z\rho/\partial_y\rho$ and h is the pycnocline depth). The ratio of vertical advection to zonal advection has the equivalent scale ϵ because of result i. Consequently, the horizontal advection terms are both largely bigger than the vertical advection one ($|u\partial_x\rho| \gg |w\partial_z\rho|$ and $|v\partial_y\rho| \gg |w\partial_z\rho|$) if the meridional length scale of the meridional density gradient l is largely smaller than the length scale associated with Earth curvature f/β, that is, $\epsilon \ll 1$. In this regime the vertical advection can be neglected and the two horizontal advections must compensate each other. Computing the scaling with the typical density field suggests that north of 35°N the vertical advection is weaker than both horizontal ones (Fig. 4; cf. section 4b for numerical values). Consistent with our analysis, Colin de Verdière and Tailleux (2005) suggested that such a regime occurs in poleward enough regions (Antarctic Circumpolar Current or North Atlantic Current) where the vertical shear of the mean flow is intense and the phase speed of large-scale baroclinic Rossby wave is reduced.

Following this scaling analysis, we formulate the hypothesis that, on first order, the steady state is a balance of the horizontal geostrophic transports. Obviously through this hypothesis we are making an error of the order of ϵ, that is, for $\epsilon > 1$ we will consider the error of the order of 1; this will be fully estimated when proceeding to numerical application (section 4b). Alternatively, the hypothesis reads

$$u_g\partial_z v_g - v_g\partial_z u_g = 0, \tag{15}$$

which corresponds strictly to the horizontal advection compensation ($u\partial_x\rho + v\partial_y\rho = 0$) under geostrophic balance. Following Bryden (1976, 1980), neglecting vertical advection suggests that the horizontal velocities are either null or their direction does not vary with depth $R^2\partial_z\phi = 0$, where $R^2 = u_g^2 + v_g^2$ is the intensity of the horizontal velocity and ϕ is an angle (measured positively anticlockwise from eastward). This means that the flow has to be a succession of unidirectional streams (but these streams could point in any direction). In the ocean at steady state, such streams' succession over the vertical are not realistic, except if it corresponds to a succession of opposite flow (e.g., a northward flow on top of a southward flow).

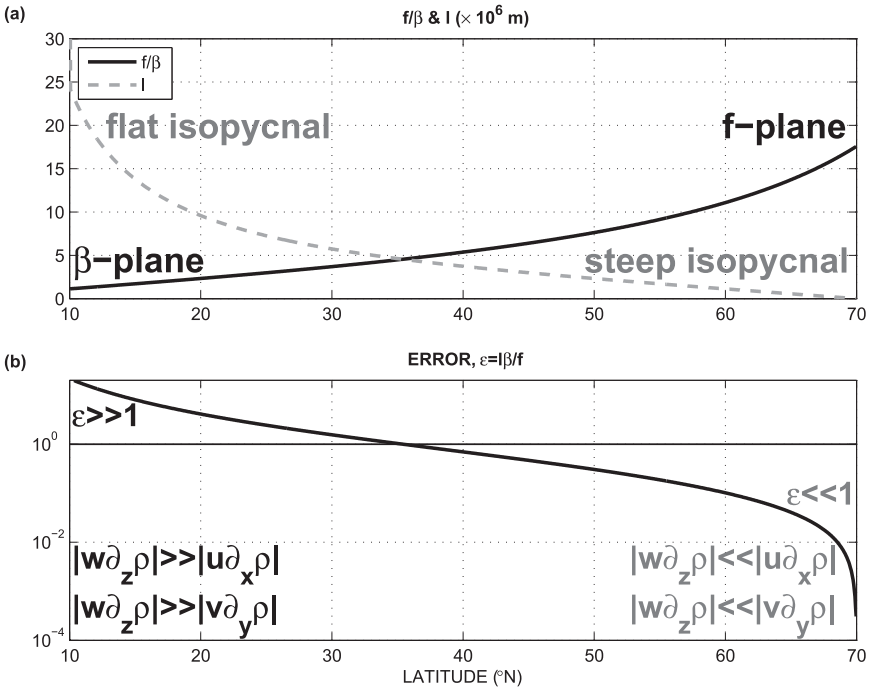

FIG. 4. (a) Meridional length scale of Earth's curvature (f/β, black solid lines) and of the meridional density gradient ($l = h\partial_z\rho/\partial_y\rho$, gray dashed lines). (b) Estimation of the relative error $\epsilon = l\beta/f$ in log scale. In the numerical application the error is considered of order 1, $O(1)$, if $\epsilon > 1$ (thin black horizontal line). The term $\epsilon \gg 1$ corresponds to a dominance of the vertical advection term over both horizontal advection ones ($|w\partial_z\rho| \gg |u\partial_x\rho|$ and $|w\partial_z\rho| \gg |v\partial_y\rho|$); $\epsilon \ll 1$ corresponds to the dominance of both horizontal advection terms over vertical advection ones ($|w\partial_z\rho| \ll |u\partial_x\rho|$ and $|w\partial_z\rho| \ll |v\partial_y\rho|$).

Vertical integration of (15) leads to a linear relation between the horizontal components of the geostrophic velocity:

$$u_g = cv_g, \tag{16}$$

where c is the ratio $(u_g/v_g)|_{z_0}$ (where z_0 is a reference depth). In other words, the ratio u_g/v_g is constant over the vertical. Because c is independent of the vertical we also have $\partial_z u_g = c\partial_z v_g$ and $\langle u_g\rangle = c\langle v_g\rangle$, where $\langle . \rangle = \int_{-H}^{0} dz/H$. This approximation of the horizontal velocities can be referred as unidirectional in the vertical since they are all aligned along the same direction. However, some authors suggest that this unidirectionality can be described as an equivalent-barotropic circulation (Killworth 1992; Killworth and Hughes 2002). This term should be used with caution to avoid misinterpretation. Actually, (16) does not prevent the horizontal velocity from having a vertical structure through horizontal density changes or even having a change in sign on the vertical or being fully compensated vertically (leading to a purely baroclinic circulation).

Friction could affect the validity of (15) and (16), especially in western boundary currents (whose contribution to the overturning circulation is significant), but north of 35°N their presence has mostly disappeared in the upper layers. Spall (1992) investigated the velocity rotation with depth in a realistic model configuration of the North Atlantic; his Fig. 1c is particularly illuminating regarding the very small rotation in large regions north of 35°N, even along the western boundary. On a more observational basis, Schott and Stommel (1978) also illustrate small rotation with depth at 55°N, 20°W in the North Atlantic Subpolar Gyre (their Fig. 2c), for instance.

Vertically integrating (12) from the bottom ($w|_{-H} = 0$) to the base of the Ekman layer [$w|_0 = -\rho_0^{-1}\partial_y(\tau_x/f)$; see section 4a for full calculations], we obtain

$$\langle v_g\rangle = -\frac{1}{\rho_0 H}\frac{f}{\beta}\partial_y\left(\frac{\tau_x}{f}\right). \tag{17}$$

Because the pressure is a potential, we have $\partial_x(fu_g) + \partial_y(fv_g) = 0$. Integrating this expression from the east (with $\langle u_g\rangle|_{x_E} = 0$) to a particular longitude and assuming that the wind is almost zonally uniform ($\tau_x \simeq \overline{\tau}_x$) we obtain

$$\langle u_g\rangle = \frac{x - x_E}{\rho_0 H}\left\{\left[1 + \partial_y\left(\frac{f}{\beta}\right)\right]\partial_y\left(\frac{\overline{\tau}_x}{f}\right) + \frac{f}{\beta}\partial_y^2\left(\frac{\overline{\tau}_x}{f}\right)\right\}. \tag{18}$$

It is interesting to note that the integration direction (as well as the no flow assumption at the eastern side of the geostrophic interior) is not innocuous; it controls the sign of c in (16) and so also controls the sign of the meridional circulation direction. Two main arguments exist in the literature to start the integration from the east. From an observational perspective, one could argue that gyre circulation has a boundary at the west with an important exchange of mass between the western boundary layer and the geostrophic interior region (Koltermann et al. 2011). In comparison, the exchange between the eastern boundary layer and the geostrophic region is rather weak. From a more dynamical perspective, one could argue that to conserve vorticity, a water mass should come from the western boundary layer to compensate the Sverdrup flow (Vallis 2006). In this study we suggest a new argument based on an energetic perspective. The no flow assumption to the east implies that the meridional geostrophic flow advection reduces potential energy. With this assumption, as it will be fully demonstrated later (section 4a), the circulation is proportional to the meridional density gradient, such that the associated density advection will reduce the meridional density gradient. On the other hand, using a no flow assumption to the west instead of the east leads to the opposite solution for c, such that the density-induced circulation ultimately increases potential energy. In other words, the western instead of eastern boundary current is consistent with a system going toward a minimum of potential energy (see section 5 for more extensive discussion).

Zonally averaging (18) provides

$$\langle \overline{u}_g \rangle = -\frac{W}{2\rho_0 H}\left\{\left[1+\partial_y\left(\frac{f}{\beta}\right)\right]\partial_y\left(\frac{\overline{\tau}_x}{f}\right)+\frac{f}{\beta}\partial_y^2\left(\frac{\overline{\tau}_x}{f}\right)\right\}. \quad (19)$$

Since the barotropic meridional flow is only a function of the zonal wind stress, also zonally uniform, $\langle \overline{v}_g \rangle = \langle v_g \rangle$. Using $\overline{c}\langle \overline{v}_g \rangle = \langle \overline{u}_g \rangle$, we obtain

$$\overline{c} = \frac{W}{2}\left\{\frac{\beta}{f}\left[1+\partial_y\left(\frac{f}{\beta}\right)\right]+\frac{\partial_y^2(\overline{\tau}_x/f)}{\partial_y(\overline{\tau}_x/f)}\right\}. \quad (20)$$

This last equation describes the coefficient $\overline{c}$ as the sum of a term independent of the wind (only a function of Earth's rotation rate and curvature) and a wind-dependent term. Because of the linearity of the final solution [fully derived later and described in (27a)], this also implies that the meridional circulation is a sum of two terms. The circulation induced by the wind-dependent term of $\overline{c}$ is highly variable along the meridional direction with unrealistic values and does not fit with state-of-the-art knowledge of the AMOC. In the rest of the study we will only focus on the wind-independent term, that is, neglecting the wind-dependent part of the last equation [or solving for a particular case, where the shape of the wind is such that $\partial_y^2(\overline{\tau}_x/f) = 0$]. So, independently of wind, we obtain an approximation for the proportionality coefficient:

$$\overline{c} = \frac{W}{2}\frac{\beta}{f}[1+\partial_y(f/\beta)]. \quad (21)$$

In general, $c = -\partial_y P/\partial_x P = dx/dy|_{P=\text{cst}}$, that is, the horizontal angle of the isobar. Before zonal averaging, this angle could be approximated by $c = -(x - x_E)(\beta/f)[1 + \partial_y(f/\beta)]$. This equation shows that the flow, along its eastward path, will slowly rotate northward, starting at an almost perfectly eastward direction at the limit of the western boundary layer and the geostrophic interior ($c|_{x_{W/I}} = 2\overline{c}$) and finishing with a purely northward flow at the limit of the eastern boundary layer and the geostrophic interior ($c|_{x_{I/E}} = 0$, allowing no zonal exchange at this location).

This angle, when zonally averaged, varies with the zonal basin extent and inversely with the Coriolis parameter, consistent with empirical discussions of Wright and Stocker (1991, 1992). This coefficient varies also with the relative meridional change of the relative meridional change of the Coriolis parameter $[\partial_y(f/\beta)/(f/\beta)]$. Since we imposed the zonal basin extent as a constant, it means that the isopycnal angle varies only because of the variation of the Coriolis parameter (i.e., Earth curvature). This implies a maximum of the angle of $\sim\pi/4$ at $\sim$55°N, the region of the North Atlantic Current (Fig. 5). In this region, our analysis shows that the meridional flow almost equates the zonal one. In the Pacific, where the zonal basin extent is up to 5 times as big as in the Atlantic, such a maximum angle would be insignificant (i.e., the flow would be primarily zonal). The mean value of the zonally averaged coefficient is 1.3 (with a standard deviation of 0.6) and 0.95 (with a standard deviation of less than 0.1) north of 35°N (location of the validity of our previous assumption). This validates, a posteriori, the use of 1 as the proportionality coefficient in the zonally averaged model of the thermohaline circulation for the Atlantic (Sévellec et al. 2006).

The last assumption is that the meridional geostrophic velocities are zonally uniform ($\overline{v}_g \simeq v_g$). For the barotropic term, it is a consequence of wind stresses being mainly zonal (Sverdrup 1947), given the cylindrical symmetry of the atmosphere because of Earth's rotation. If vertical shear exists ($\partial_z v \neq 0$), we have $\partial_x \rho \simeq (\rho|_{x_E} - \rho|_{x_W})/W$, implying that the zonal density gradient is constant. (This last approximation is equivalent to $\overline{\rho} - \rho|_{x_W} = \rho|_{x_E} - \overline{\rho}$.) Using this last assumption together with (13) and (21), we have a relation between

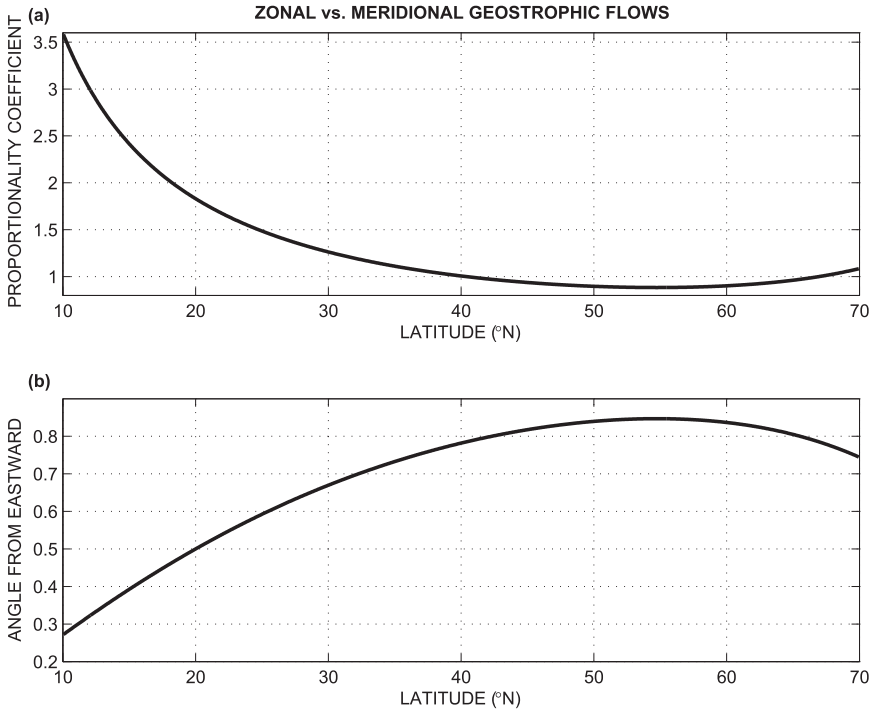

FIG. 5. (a) Zonally averaged proportionality coefficient between the zonal and meridional geostrophic velocities: $\bar{c} = \bar{u}_g/\bar{v}_g$. (b) Angle of the geostrophic flow (radians measured from eastward; a value of $\pi/2$ corresponds to a northward flow). The approximate solution is only valid north of 35°N.

the eastern–western density difference and the meridional density gradient:

$$\rho|_{x_E} - \rho|_{x_W} = -\frac{2}{\frac{\beta}{f}[1 + \partial_y(f/\beta)]}\partial_y\overline{\rho}. \qquad (22)$$

Applying this relation to (10b) allows us to estimate the vertical shear of the meridional velocity from the meridional gradient of density. This is sufficient to consistently close the set of equations of the zonally averaged ocean model.

4. The general solution and application

a. The general solution

From (10b) we can link the zonal density difference to the vertical shear of meridional velocity. Assuming that one knows the density field, the circulation can be obtained under a constraint on the velocity on the vertical (either a value at a particular depth or vertical integral properties). The equation we have not used so far is the nondivergence in its zonally averaged form [(7)]. After vertical integration we obtain $\int_{-H}^{0}\partial_y\overline{v}\,dz + \overline{w}|_0 = 0$ (assuming no vertical flow at the bottom of the ocean $\overline{w}|_{-H} = 0$). After meridional integration, and assuming the existence of a solid wall at a particular latitude ($\overline{v}|_{y_1} = 0$, where y_1 is the latitude of the solid wall), we obtain

$$\int_{-H}^{0}\overline{v}\,dz - \int_{y}^{y_1}\overline{w}|_0\,dy = 0. \qquad (23)$$

This relation corresponds to the baroclinicity condition, often used in a zonally averaged model, rectified by a vertical surface boundary condition. The wind stress and thus Ekman pumping induce a circulation distributed over the water column. Equations (10b) and (23) provide a closed system for determining the zonally averaged meridional velocity $\overline{v}$.

The boundary condition at the ocean surface ($z = 0$) can be obtained by the Ekman layer dynamics (balance between Coriolis force and the vertical viscosity; Pedlosky 1979). Thus, the flux at the base of the Ekman layer is imposed by the wind stress in the zonal direction (after assuming no transfer of momentum between the Ekman layer and the ocean interior, i.e., the ocean interior slips freely below the Ekman layer). We obtain the Ekman pumping

$$W\int_{y}^{y_1}\overline{w}|_0\,dy = -\psi|_0 = \frac{W}{f\rho_0}\overline{\tau}_x, \qquad (24)$$

where $\overline{\tau}_x$ is the zonally averaged zonal wind stress and ψ is the streamfunction such that $\partial_z\psi = -W\overline{v}$ and $\partial_y\psi = W\overline{w}$. Here, we have also neglected the eastern–western difference of meridional wind stress: $(\tau_y|_{x_E} - \tau_y|_{x_W})/W \ll \partial_y\overline{\tau}_x$. This assumption is consistent with the solid boundary condition at the zonal edges of the basin, and so is consistent with mass conservation of the Ekman layer. We stress that, within this formulation, the streamfunction at the surface is not restricted to zero since mass conservation is only obtained when both interior and Ekman transports are added. However, the use of streamfunction remains mathematically correct since the flow is nondivergent (equivalent to conservation of mass under Boussinesq approximation; Spiegel and Veronis 1960; Boussinesq 1903).

Finally integrating (10b) and applying (23) and (24) leads to

$$\overline{v} = -\frac{1}{fH\rho_0}\overline{\tau}_x + \frac{\lambda}{(f^2+\lambda^2)\rho_0}\partial_y(\overline{P} - \langle\overline{P}\rangle) - \frac{f}{(f^2+\lambda^2)\rho_0}\left[\frac{(P-\langle P\rangle)|_{x_E} - (P-\langle P\rangle)|_{x_W}}{W}\right]. \quad (25)$$

This result is equivalent to the decomposition of Hirschi and Marotzke (2007) in the context of a flat bottom.

Using $\psi|_{-H} = 0$ (no mass flux at the bottom of the ocean), we obtain

$$\psi = -\overline{\tau}_x\frac{W}{f\rho_0}\frac{z+H}{H} - \frac{\lambda W}{(f^2+\lambda^2)\rho_0}\int_{-H}^{z}\partial_y(\overline{P} - \langle\overline{P}\rangle)\,dz + \frac{f}{(f^2+\lambda^2)\rho_0}\int_{-H}^{z}\left[(P-\langle P\rangle)|_{x_E} - (P-\langle P\rangle)|_{x_W}\right]dz. \quad (26)$$

This expression shows that the flow is both driven by the wind and by the vertical pressure anomaly (i.e., often referred to as the baroclinic pressure). Without wind stress, $\overline{\tau}_x = 0$, and in the absence of a thermocline (no stratification; $P - \langle P\rangle$ is zonally and meridionally uniform), the flow will vanish. Thus, the so-called thermohaline circulation is the terms related to the baroclinic pressure on the right-hand side of (25) or (26).

Despite the fact that the results obtained are extremely useful to understand the drivers of the AMOC, it refers to the eastern–western baroclinic pressure difference to drive the AMOC. As it stands, it is useless in the context of a zonally averaged model of the AMOC. However, using the closure from section 3c, that is, (22), showing a local link between the eastern–western density difference and the meridional density gradient, allows us to define the AMOC dynamics in a purely zonally averaged framework. Using (22), we express (26) as

$$\psi = -\overline{\tau}_x\frac{W}{f\rho_0}\frac{z+H}{H} - \frac{\lambda W + 2f^2/\{\beta[1+\partial_y(f/\beta)]\}}{(f^2+\lambda^2)\rho_0}\int_{-H}^{z}\partial_y(\overline{P} - \langle\overline{P}\rangle)\,dz, \quad \text{and} \quad (27a)$$

$$\simeq -\overline{\tau}_x\frac{W}{f\rho_0}\frac{z+H}{H} - \frac{2}{\rho_0\beta[1+\partial_y(f/\beta)]}\int_{-H}^{z}\partial_y(\overline{P} - \langle\overline{P}\rangle)\,dz. \quad (27b)$$

It is interesting to note that the smallness of friction ($\lambda \ll f$) makes the thermohaline mass transport independent of the size of the basin, in contrast to the wind-driven part. Equation (27b) is independent of friction (except to convey the momentum transfer by the wind). In contrast to previous zonally averaged closure (e.g., Marotzke et al. 1988; Wright et al. 1995), the solution is derived here from a purely geostrophic circulation.

We now have a relation between the thermohaline part of the meridional flow and the meridional baroclinic pressure gradients, without any need for parameterization. Thus, this theoretical relation can be directly implemented in zonally averaged ocean models to study, for example, AMOC hysteresis (Sévellec and Fedorov 2011).

b. Application

To test the validity of our solution we will apply it on an idealized synthetic stratification and surface wind forcing of the ocean. For discussion, and given the linearity of our set of equations, we do not only solve the full problem but we also decompose the solution in the three forcing terms: temperature, salinity, wind. Using the synthetic surface momentum forcing and density field defined in section 2c, expressing the circulation does not present any particular difficulty.

Deriving the solution from (27a) leads to $\psi = \psi_T + \psi_S + \psi_W$, with

$$\psi_T = \frac{\pi}{2}\frac{\alpha_T g\Delta T h^2}{(f^2+\lambda^2)LH}\left\{\lambda W + \frac{2f^2}{\beta[1+\partial_y(f/\beta)]}\right\} \times\left[(1-e^{-H/h})\frac{z}{h} + 1 - e^{z/h}\right]\sin\left(\frac{\pi}{2}\frac{y-y_0}{y_1-y_0}\right), \quad (28a)$$

$$\psi_S = \pi\frac{\alpha_S g\Delta S h^2}{(f^2+\lambda^2)LH}\left\{\lambda W + \frac{2f^2}{\beta[1+\partial_y(f/\beta)]}\right\} \times\left[(1-e^{-H/h})\frac{z}{h} + 1 - e^{z/h}\right]\cos\left(\pi\frac{y-y_0}{y_1-y_0}\right), \quad \text{and} \quad (28b)$$

$$\psi_W = \frac{\tau_x^0 W}{\rho_0}\frac{z+H}{H}\sin\left(2\pi\frac{y-y_0}{y_1-y_0}\right), \quad (28c)$$

where ψ_T, ψ_S, and ψ_W are the circulation components due to the temperature field, the salinity field, and the wind stress forcing, respectively; $L = \pi R_E(y_1 - y_0)/180$ is the meridional extent of the basin, and R_E is Earth's radius.

The thermally induced circulation corresponds to a northward flow at the surface and a broad return flow at depth (Fig. 6a). This thermally induced circulation has a single cell, whereas the salinity-induced circulation has two cells as well as the wind-driven one. The salinity partially reduces the thermal circulation between 40° and 70°N but intensifies the thermal cell from 10° to 40°N (Fig. 6b). The wind cells intensify the circulation south of 40°N and reduce it in the north (Fig. 6c). This reduction is visible on the total circulation by the shallow negative cell located in the first 100 m around 55°N. Overall, the circulation shows a local maxima of ~18 Sverdrups (Sv; 1 Sv $\equiv 10^6\,\mathrm{m^3\,s^{-1}}$) at 30°N (Fig. 6d).

Since the flow was determined as an approximation, based on a scaling approach, one should also consider the error made on the solution. Consistently with the scaling analysis, this error is of the same order as ϵ, setting it to $\pm\epsilon$ times the solution. To acknowledge the limitation of our hypothesis, for $\epsilon > 1$ we set the error to the order of 1, with the symbol $\pm O(1)$. Thus, the circulation intensity at 30°N corresponds to 18 $\pm O(1)$ Sv. This intensity of the flow could be compared with 18 ± 5 Sv from Talley et al. (2003) or 24 ± 2.4 Sv from the rapid section at 26.5°N (Cunningham et al. 2007). A recent inverse model study suggests 18.0 ± 2.5 Sv at 24°N, 16.3 ± 2.7 Sv at 48°N, and 17.0 ± 4.3 Sv at 56°N (Lumpkin and Speer 2007). At these two last locations our idealized model shows values of 14 ± 5.1 Sv and 13 ± 2.2 Sv, respectively. The idealized model shows a mass transport consistent with oceanic measurements.

For the thermally induced circulation the vertical maximum of the streamfunction occurs at $\partial_z \psi_T = 0$:

$$z_{\max} = h \ln\left[\frac{h}{H}(1 - e^{-H/h})\right], \tag{29}$$

where $z_{\max}$ is the vertical location of the maximum (vertical line in Fig. 6a). The maximum of the circulation is given by

$$\psi_{\max} = \frac{\pi}{2}\frac{\alpha g \Delta T h^2}{(f^2+\lambda^2)LH}\left\{\lambda W + \frac{2f^2}{\beta[1+\partial_y(f/\beta)]}\right\} \times\left\{(1-e^{-H/h})\frac{h}{H}\ln\left[\frac{h}{H}(1-e^{-H/h})\right] - \frac{h}{H}(1-e^{-H/h}) + 1\right\}, \tag{30}$$

where $\psi_{\max} = \psi|_{z_{\max}}$. This result shows that if the thermocline depth decreases ($h \to 0$), the location of the maximum streamfunction also decreases ($z_{\max} \to 0$) as does the intensity of the circulation ($\psi_{\max} \to 0$). So, in a consistent manner with the Sandström (1908) experiments, in the absence of mixing ($h = 0$) and wind, the circulation vanishes. Note that in a purely Lagrangian numerical model where there is no diabatic mixing, there exists a ''chaotic'' mixing setting a stratification and thus allowing the circulation (Haertel and Fedorov 2012).

A key feature of the AMOC is its inherent global scale. From (26), which did not use the closure, we can see that it derives from the density field, that is, the interhemispheric nature of the AMOC comes from the interhemispheric nature of the density field. This means that any remote effect, such as the effect of Southern Ocean wind, modifies the AMOC through a modification of the density field. It is even clearer from (30), where the intensity of the circulation is modulated by the thermocline depth. Thus, the Southern Ocean westerlies or any vertical mixing processes can and will remotely impact the AMOC intensity by modifying the thermocline depth.

Our set of equations does not only allow us to estimate the meridional overturning streamfunction but also the zonally averaged zonal velocities, using (10a) to determine the baroclinic part of the flow, together with (19) to determine its barotropic part. South of 45°N, the flow is eastward above ~1000 m and westward below (Fig. 7d). North of 45°N, the flow is purely eastward, with a maximum intensity around 60°N. The thermally induced velocity field shows the dominance of the eastward flow above ~1500 m and westward flow below (Fig. 7a). This depth corresponds to $z_{\max}$, showing that the level of no motion is the same for zonal and meridional flow. The baroclinic part of the flow is dominated by the thermally induced term (Fig. 7a vs 7b), whereas the barotropic component is driven by the wind stress (Fig. 7d). The maximum velocities appear at the surface, slightly below $1\,\mathrm{cm\,s^{-1}}$.

We can also look at the meridional heat transport defined by

$$\mathrm{MHT} = W\rho_0 C_p \int_{-H}^{0} \overline{v}\,\overline{T}\,dz, \tag{31}$$

where C_p is the heat capacity of seawater. Note that this expression of meridional heat transport is approximate since the meridional heat transport should be the vertical integral of $\overline{vT}$ (see discussion in section 3a for more extensive comments).

This meridional heat transport peaks around 1.1 ± $O(1)$ PW at 25°N [Fig. 8a, where we assumed (as for the

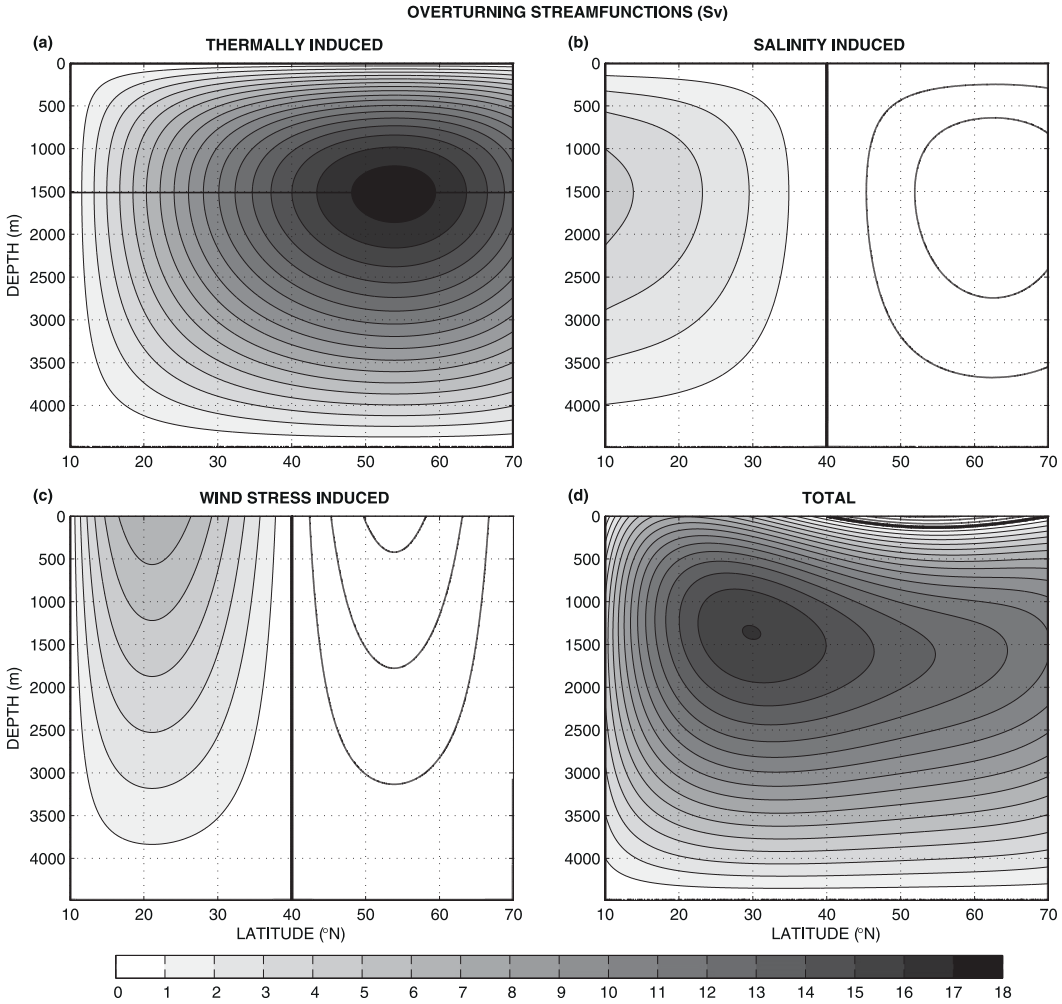

FIG. 6. Streamfunction of the Atlantic meridional overturning circulation (Sv). Solutions of the (a) thermally, (b) salinity-, and (c) wind-induced circulation, summing up to the (d) full solution (including temperature, salinity, and wind). Grayscale shading is superimposed on the contours for positive values (following the white-to-black color bar scale). Negative values are shown by contours without the white-to-black shading superimposed. Contour interval is 1 Sv. Positive values denote clockwise circulation. The horizontal black line in (a) denotes the depth of the maximum of the streamfunction, following (30). The (a) thermal and (b) haline approximate solutions, as well as the thermohaline component of the total solution in (d), are only valid north of 35°N.

mass transport) that the solution is an approximation with a relative error bar of $\pm\epsilon$ of the solution, and $O(1)$ corresponds to $\epsilon > 1$]. These two values are typical of heat transport in the ocean (e.g., 1.3 PW at 24°N; Ganachaud and Wunsch 2000). At the same location, Lumpkin and Speer (2007) estimate the heat transport as 1.25 ± 0.25 PW and 0.61 ± 0.11 PW at 48°N and 0.54 ± 0.11 PW at 56°N. At these two last locations our idealized model has heat transports of 0.4 ± 0.15 PW and 0.25 ± 0.04 PW, respectively. The idealized model shows heat transport consistent with oceanic measurements.

The transport is dominated by the wind-driven term below 30°N (Fig. 8a). Since there is no methodological error bar for the wind-driven circulation (i.e., no closure is required), this partially explains the good accuracy of heat transport at low latitude (where our approximation is the worst; cf. Fig. 4). The thermally induced transport dominates elsewhere. The salinity component of the circulation is only important south of 15°N.

In the same way we can define the meridional freshwater transport:

$$\mathrm{MFT} = -\frac{W}{S_0}\int_{-H}^{0} \overline{v}\,\overline{S}\,dz, \tag{32}$$

where S_0 is the reference salinity. (As previously, this term is an estimate since freshwater transport should derive from the vertical integral of $\overline{vS}$.)

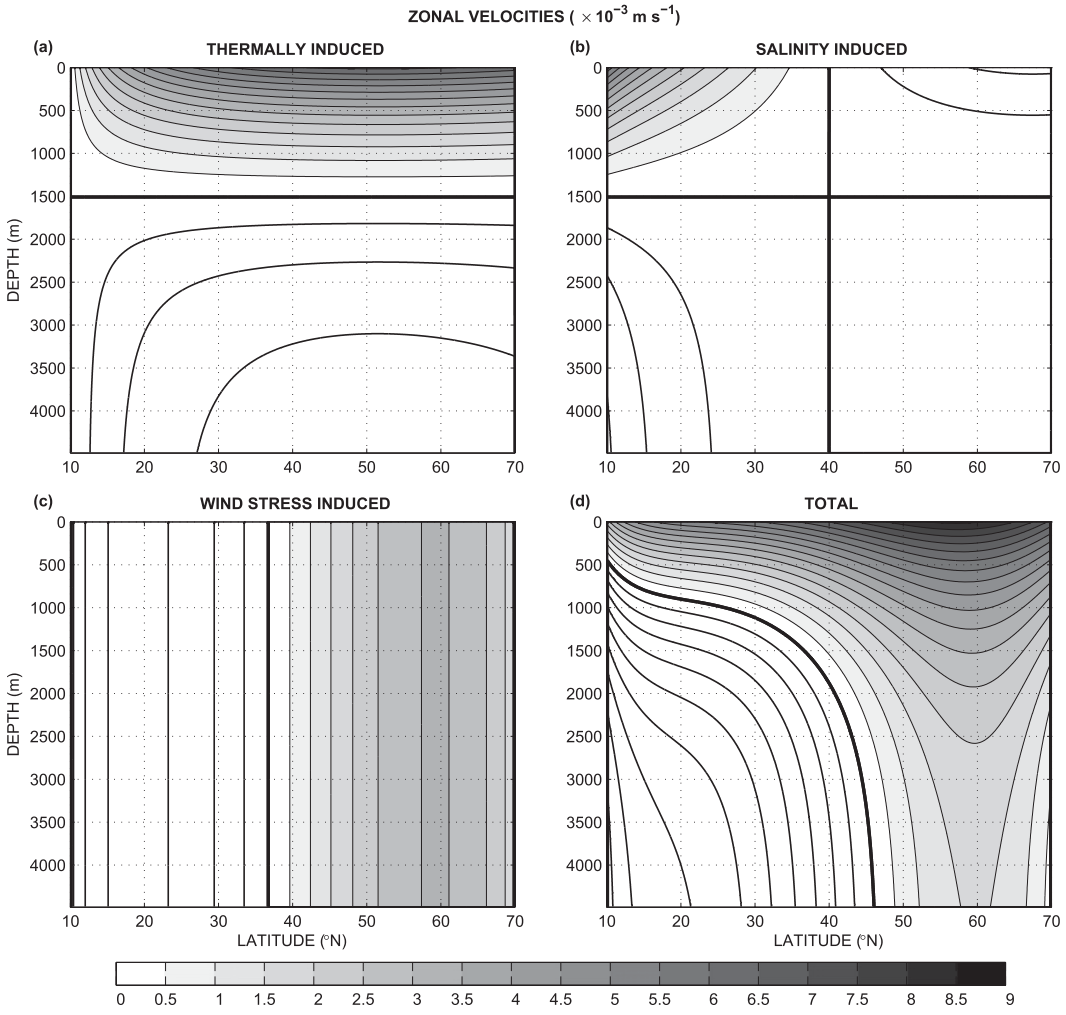

FIG. 7. As in Fig. 6, but for the zonally averaged zonal velocities ($\times 10^{-3}$ m s^{-1}). Positive values denote eastward flow (shaded according to the color bar). Negative values (westward) are not shaded. Zero contour is bold. Contour interval is 0.5×10^{-3} m s^{-1}.

The freshwater transport is consistent with evaporation in the southern part of the North Atlantic and precipitation north of 35°N (Fig. 8b). Since we do not specify the surface freshwater flux, this diagnostic is especially useful to test the accuracy of the circulation relative to the stratification.

5. Discussion

In this study, we suggest that zonally averaged ocean models represent the ocean dynamics under four main assumptions that restrict their validity:

1) The obvious main approximation of such study is the 2D (latitude-depth) vision of the ocean circulation. In this context, mass, heat, and freshwater are transported through the meridional overturning circulation (rather than through the horizontal, eddy and/or gyres, circulation).
2) The momentum equations are assumed at steady state and correspond to low Rossby number with a limited parameterization of the momentum dissipation through Rayleigh friction (vertical viscosity being treated in appendix B).
3) A vertical unidirectionality of the horizontal flow was hypothesized and its error estimated (i.e., the horizontal flow is aligned along a single direction all over the vertical). This results from the density advection balance at equilibrium when the meridional density gradient length scale is shorter than Earth's curvature length scale (equivalent to the *f*-plane and quasigeostrophic approximations). This assumption holds well in regions of steep isopycnal slope, such as the North Atlantic Current, that is, north of 35°N.

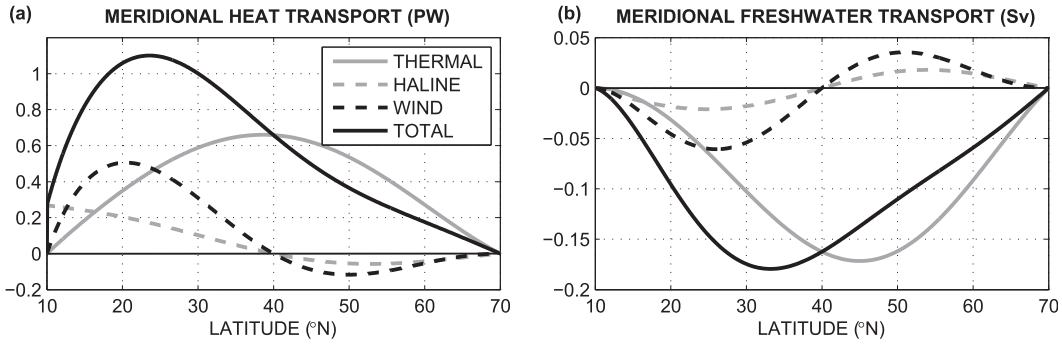

FIG. 8. Meridional transport of (a) heat and (b) freshwater decomposed in their three forcing components: thermal, haline, and wind. The thermal and haline approximate solutions, as well as the thermohaline component of the total solution, are only valid north of 35°N.

4) From these approximations we have analytically demonstrated a link between the zonally averaged meridional gradient of density and the meridional overturning circulation, if the zonal density change is linear (or the meridional velocity are zonally uniform).

This last result and its mathematical expression lead to several implications for the ocean dynamics that we will discuss.

a. Relation to existing zonally averaged circulation model

One striking result, deriving from (27a), is that the widely used linear frictional dependence of the meridional flow to meridional pressure gradient is actually achieved. The solution of (27a) reinforces, a posteriori, the use of such parameterization extensively applied in zonally averaged ocean models (Wright and Stocker 1991, 1992; Sévellec et al. 2006, 2010; Sévellec and Fedorov 2011; Colin de Verdière et al. 2006; Colin de Verdière and te Raa 2010). This suggests that the zonally averaged circulation is actually driven by the meridional pressure gradient in the northern region.

Our analysis requires oceanic latitudinal bands to be in steady state. It is natural to state that such steady state is achieved only after both barotropic and baroclinic waves have adjusted the eastern–western pressure gradient (Johnson and Marshall 2002). One can thus consider that relation between meridional density gradient and the AMOC [(27a)] is valid on longer time scales than this zonal adjustment. We estimate that such zonally averaged ocean models are useful to study the AMOC on time scales longer than the decades, for example, centennial and millennial variability or steady state.

However, our scaling approach does not allow discussion of the planetary scale; as mentioned earlier, the assumption is accurate only north of 35°N. This suggests that, for instance, the Stommel (1961) two-box model, as a representation of the thermohaline circulation (e.g., Huang 2010), describes only the northern part of the North Atlantic. Thus, although they are still a radical reduction of the zonally averaged ocean model, our study validates the use of box models or loop models to coarsely represent the northern region of the AMOC as suggested by the pioneer visions of Stommel (1961), Howard (1971), and Malkus (1972), as long as the time scales investigated are sufficiently long.

More broadly, this suggests that the bistability behavior of the AMOC, derived from the Stommel (1961) model, should be restricted to northern North Atlantic phenomena. Thus, paleoclimate study, using meridional density gradient changes to explain past AMOC reorganizations (e.g., Broecker et al. 1990), should be regarded as a local explanation (not global pole to pole). This does not mean that AMOC reorganization is not a global phenomenon, but a more sophisticated argument than simple meridional density changes is required.

b. Relation to available potential energy

On the one hand, following (27a), the meridional flow is induced by a gradient of density $\partial_y \overline{\rho}$. On the other hand, 2D divergence of the flow ($\partial_y \overline{v} + \partial_z \overline{w} = 0$) shows that the vertical flow is driven by meridional divergence of the meridional flow. These two elements act to reduce the available potential energy (APE) (Fig. 9). This suggests that our geostrophic closure of zonally averaged ocean model leads the system toward a minimum of potential energy [consistent with the analysis of Sijp et al. (2012)].

In the absence of APE, source the circulation will slowly reduce APE and at the same time vanish. This means that the circulation is sustained only if a source of APE exists in the system. This is consistent with the Sandström (1908) experiment; using heating and cooling at the same geopotential (the ocean surface) and with no

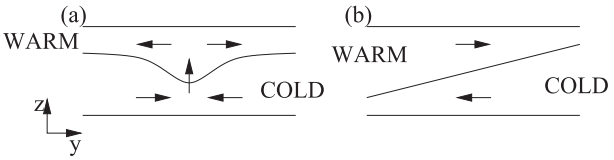

FIG. 9. Schematic view of the circulation induced by (a) a Gaussian anomaly or (b) a linear slope of the isopycnals (y and z are the meridional and vertical coordinates, respectively). In both cases the circulation tends to remove the excess of available potential energy by flattening the isopycnal slope.

external source of mechanical energy (absence of mixing), the circulation vanishes (Huang and Wang 2003).

c. *Atlantic versus Pacific*

From (27b), we see that the thermohaline part of the AMOC is independent of the zonal basin extent, whereas the wind-driven part is proportional to this zonal basin extent. Hence, the relative contribution of the wind-driven circulation will increase in a wider basin. For the exact same stratification as the one we used, the North Pacific Ocean (up to 5 times as wide as the Atlantic Ocean) will show a radically different zonally averaged circulation: almost no circulation in the north (north of 50°N, the wind-driven cell strongly reducing the thermohaline circulation) and an intense cell in the south (almost ~50 Sv south of 50°N). This potentially explains the absence of deep-water formation in the North Pacific. The importance of the zonal extent to exhibit Atlantic-like or Pacific-like circulation has also been suggested by Ferreira et al. (2010) in an idealized configuration of a coupled atmosphere–ocean–ice model.

This change in the dynamics of the meridional overturning circulation between the Atlantic and the Pacific is related to the angle between the zonal and the meridional geostrophic flows. Equation (21) transformed a purely eastward geostrophic flow (the ocean density being primarily forced by the north–south heating difference) in an eastward flow with a northward component. However, this angle is proportional to the zonal basin extent. For a wider basin the regime is more zonal, that is, the angle peaks at ~55°N with a value of ~45° in the Atlantic and only ~9° in the Pacific (angles are measured counterclockwise from the east). A wider basin requires a smaller counterclockwise rotation of the eastward geostrophic flow to achieve no zonal flow at the eastern boundary. This rotation mechanism could explain the existence of the North Atlantic drift and the absence of such phenomenon in the Pacific. Also, for the same reason, the zonal gradient of sea surface temperature is stronger in the Atlantic than in the Pacific, so one should expect higher northward surface wind in the Atlantic than in the Pacific, leading to more intense northward atmospheric heat transport and so a milder climate on its eastern border (i.e., Europe vs Canada).

To summarize, even if the northern–southern heating difference is primarily the same between the Atlantic and Pacific, the zonal basin extent difference, together with (21), suggests the absence of thermohaline circulation and explains the primarily zonal dynamics in the Pacific compared to the Atlantic. That is, the zonal basin extent of the Atlantic is a key aspect for the existence of both thermohaline circulation and North Atlantic Current. This suggests a greater propensity for deep-water formation in the North Atlantic than in the North Pacific and gives an additional argument to justify the maintenance of a stronger overturning in the Atlantic compared to the Pacific.

6. Conclusions

The link between the AMOC and meridional density gradient has been assumed in a wide range of climate and oceanic analyses (going from water-hosing experiments to thermohaline circulation hysteresis). This relation has been extensively used in zonally averaged ocean models. It is also the cornerstone of the impact of Arctic meltdown on the AMOC, that is, a massive freshening of the North Atlantic could shut down the AMOC and hence alter climate. Despite being convenient and empirically plausible, this relation has never been rigorously demonstrated.

In this study we have analytically related the AMOC strength to the meridional density gradient (more precisely the meridional baroclinic pressure gradient). We show that the former is proportional to the latter. The proportionality coefficient is related to Earth's curvature and its rotation (i.e., the Coriolis parameter and its meridional derivatives). Unlike previous studies (Marotzke et al. 1988; Wright and Stocker 1991; Wright et al. 1995), this solution does not require any parameterization. Our solution can be analytically derived from the classical planetary-geostrophic set of equations under few assumptions, which could be and have been tested.

This methodology is particularly useful since it gives an estimate of the error on our result and thus suggests a limit to the use of zonally averaged ocean models. We obtain that these models are valid to represent the North Atlantic north of 35°N, where the meridional length scale of isopycnal outcropping is much smaller than the Earth radius. Also, building on steady-state equations, the isopycnals must have adjusted to the basinwide forcing, such that the use of zonally averaged ocean models are restricted to study time scales longer than decades.

This result has also several implications that we discussed in this study. Using the momentum equation we can accurately separate the wind-induced circulation and the thermohaline circulation (driven by both temperature and salinity), the latter necessarily pushing the system toward a minimum of APE. The form of the proportionality coefficient leads to a more intense North Atlantic Current than its Pacific equivalent (because the latter basin is wider than the former).

From our analysis, we have also shown that the AMOC exhibits two regimes. They can be differentiated from the main balance in the density evolution, horizontal versus vertical advection [consistently with the analysis of Colin de Verdière and Tailleux (2005)]. The regime is determined by the ratio of the meridional length scale of isopycnal outcropping to Earth's radius. It roughly corresponds to the northern and southern part of the North Atlantic. Only the former regime has been studied here, and the solution presented here is not valid for the latter. This latter regime is more favorable to large-scale baroclinic Rossby waves. It is characterized by a more dominant role of the vertical advection term (vs the horizontal advection terms) to equilibrate the evolution of tracers.

In the framework of our study, where the density is assumed to be known, the zonally averaged circulation is a local diagnostic of the density field. This means that the intrinsic global and interhemispheric nature of the AMOC is given by the density field. In particular the isopycnal depth, which is partially set by Southern Ocean processes (Gnanadesikan 1999; Wolfe and Cessi 2011; Nikurashin and Vallis 2012), participates in setting the intensity of the flow [(29) and (30)]. In this context Southern Ocean processes, as well as other remote processes (global vertical mixing), influence the intensity of the AMOC by actively setting the North Atlantic density field.

In the limit of validity of our closure, north of 35°N, our results suggest that the outcropping region in the North Atlantic is concomitant with a downwelling of water. Because of mass conservation this water has to upwell in others regions. The two mains candidates for this upwelling are through global vertical mixing or the interaction between the wind-driven circulation and the eddy-induced circulation in the Southern Ocean. Whereas the latter is often suggested in recent description of the AMOC (e.g., Gnanadesikan 1999; Haertel and Fedorov 2012), the former remains a valid hypothesis that can enhance or participate in the total upwelling (Sévellec and Fedorov 2011). Both hypotheses cannot be represented by our suggested closure, since the Southern Ocean is zonally periodic and the subtropical region has flat isopycnals. Note that based on our scaling (Fig. 4), the flat isopycnals in the subtropical region are consistent with a region of strong vertical upwelling [$w\partial_z\rho = \partial_z(k_z\partial_z\rho)$] versus horizontal advection and so also are consistent with the theory of deep-ocean circulation (Stommel 1958; Stommel and Arons 1960a,b), where vertical upwelling induces an abyssal circulation.

Numerical models using zonally averaged closure were shown to accurately reproduce water mass properties in the entire Atlantic (e.g., Knutti et al. 2000; Sévellec and Fedorov 2011). However, as discussed above, AMOC in tropical region is in a different regime than the one used in our demonstration. In the Southern Ocean, AMOC is also in a different regime because of the periodic zonal boundary conditions. Thus, if a link still exists between the zonal and meridional density gradient in the tropical region and Southern Ocean, this link needs to be demonstrated in a different way. This will be the goal of future investigations.

Acknowledgments. This research was supported by the Natural and Environmental Research Council United Kingdom (MESO-CLIP, NE/K005928/1) and by the Ti Ammo project funded through the French CNRS/INSU/LEFE program. We thank Alain Colin de Verdière, Rémi Tailleux, and Kevin Oliver for sharing their insight on the AMOC dynamics that improved earlier versions of the manuscript. We also thank the editor, Michael Spall, and two anonymous reviewers for their useful comments that helped us clarify the manuscript.

APPENDIX A

Momentum Equations and Boundary Conditions

We will demonstrate that, depending on the form of the momentum equations together with the choice of boundary condition, the density difference, typical of geostrophic flow, could not drive a zonally averaged meridional flow. For this we will use the boundary condition in a 3D field and show that the consequences are fundamental for the 2D dynamics (i.e., zonally averaged).

a. Rigid boundary in a geostrophic model

Rewriting (9a) and (9b), in the absence of friction, as a normal and a tangential term to a local boundary,

$$-f\partial_z u_s = \frac{g}{\rho_0}\partial_n\rho, \quad \text{and} \tag{A1a}$$

$$f\partial_z u_n = \frac{g}{\rho_0}\partial_s\rho, \tag{A1b}$$

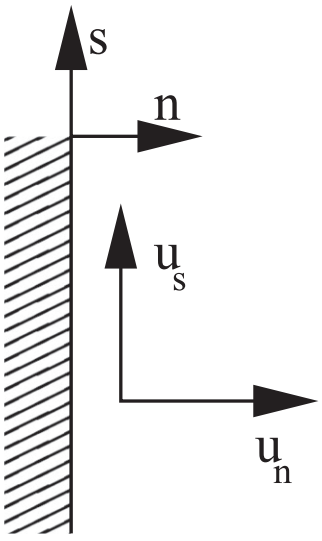

FIG. A1. Tangential and normal coordinates along a solid boundary and their respective velocities. Dashed region represents the boundary with adiabatic ($\partial_n\rho|_{n=0} = 0$) and/or solid ($u_n|_{n=0} = 0$) conditions.

where s and n are the tangential and normal coordinates, and u_s and u_n are the tangential and normal velocities (Fig. A1).

At the boundary ($n = 0$) we impose a rigid boundary (i.e., no mass flow, $u_n|_{n=0} = 0$). Applying this boundary condition, we have from (A1b) $\partial_s\rho|_{n=0} = 0$. This shows that the density along the boundary $\rho|_{n=0}$ is constant. Thus, to be consistent with geostrophic equations, the density field is always adjusted along a solid boundary.

In the context of the North Atlantic, the existence of a northern boundary in idealized configuration, connecting the eastern to the western boundaries, induces that the density along these boundaries should be equal ($\rho_{x_W} = \rho_{x_E}$). However, we stress that the existence of such a northern boundary is a shortcoming of the actual topography.

This implies that the zonally averaged geostrophic flow, proportional to the difference in density between the east and west, should vanish. This suggests that the geostrophic balance alone is inconsistent with mass conservation.

b. *Solid boundary in a geostrophic model with Rayleigh friction*

We rewrite (9a) and (9b) as a normal and a tangential term:

$$-f\partial_z u_s = \frac{g}{\rho_0}\partial_n\rho - \lambda\partial_z u_n, \quad \text{and} \tag{A2a}$$

$$f\partial_z u_n = \frac{g}{\rho_0}\partial_s\rho - \lambda\partial_z u_s. \tag{A2b}$$

At the boundary ($n = 0$) we have no normal flux of mass and heat ($\partial_n\rho|_{n=0} = 0$ and $u_n|_{n=0} = 0$). Applying this boundary condition, we have from (A2a) $\partial_z u_s|_{n=0} = 0$ and from (A2b) $\partial_s\rho|_{n=0} = 0$. The latter showing that the density along the boundary $\rho|_{n=0}$ is constant. Thus, in a geostrophic system with Rayleigh friction, the density is always adjusted along a solid boundary.

This implies that the zonally averaged geostrophic flow, proportional to the difference of density between the east and west, should vanish. This suggests that the geostrophic balance plus Rayleigh friction is inconsistent with mass and heat conservations.

APPENDIX B

The Explicit Surface Boundary Layer Case

In the main part of the manuscript we have imposed an Ekman layer on top of the ocean. Here, we will explicitly solve the vertical boundary layers (by adding a vertical viscosity in the momentum equations). We will demonstrate that it leads to the same circulation in the interior and a boundary layer controlled by two different vertical scales (both linked to the Ekman layer thickness).

Starting from the momentum equations in (1) and incorporating a vertical Laplacian viscosity, we have

$$-fv = -\frac{1}{\rho_0}\partial_x P - \lambda u + \nu\partial_z^2 u, \quad \text{and} \tag{B1a}$$

$$fu = -\frac{1}{\rho_0}\partial_y P - \lambda v + \nu\partial_z^2 v, \tag{B1b}$$

where ν is the vertical eddy viscosity coefficient.

After vertical differentiation, and expressing these equations in their zonally averaged form, we obtain

$$[f^2 + (\lambda - \nu\partial_z^2)^2]\partial_z\overline{u} = \frac{g}{\rho_0}\left[(\lambda - \nu\partial_z^2)\frac{\rho|_{x_E} - \rho|_{x_W}}{W} + f\partial_y\overline{\rho}\right],$$

and

(B2a)

$$[f^2 + (\lambda - \nu\partial_z^2)^2]\partial_z\overline{v} = \frac{g}{\rho_0}\left[(\lambda - \nu\partial_z^2)\partial_y\overline{\rho} - f\frac{\rho|_{x_E} - \rho|_{x_W}}{W}\right].$$

(B2b)

a. *Solution*

To explicitly solve (B2b), we define the vertical shear of the meridional velocity: $\mathcal{S} = \partial_z^2\psi = -W\partial_z\overline{v}$, where ψ is the meridional streamfunction. This shear is split in three terms $\mathcal{S} = \mathcal{S}_I + \mathcal{S}_S + \mathcal{S}_B$, where $\mathcal{S}_I$, $\mathcal{S}_S$, and $\mathcal{S}_B$ are the interior, surface, and bottom solutions.

1) THE INTERIOR SOLUTION

The interior solution is derived from (10b) away from the vicinity of the vertical boundary and corresponds to

$$\mathcal{S}_I = \frac{g}{(f^2+\lambda^2)\rho_0}[f(\rho|_{x_E} - \rho|_{x_W}) - \lambda W \partial_y \overline{\rho}]. \quad \text{(B3)}$$

In the absence of vertical viscosity, this last equation is strictly the same as (10b) (i.e., the equation expressed in the implicit surface boundary case, main part of the manuscript, is equivalent to $\nu = 0$). This equation relates the density gradient to the vertical shear of meridional velocity. However, in this appendix we will use a slightly more general approach than in the main part of the manuscript to determine the velocity. We will explicitly solve the surface and bottom boundary layers.

2) THE SURFACE AND BOTTOM BOUNDARY SOLUTIONS

The surface and bottom boundary condition follows

$$\frac{\nu^2}{f^2+\lambda^2}\partial_z^4 \mathcal{S}_{S/B} - 2\frac{\lambda\nu}{f^2+\lambda^2}\partial_z^2 \mathcal{S}_{S/B} + \mathcal{S}_{S/B} = 0. \quad \text{(B4)}$$

These fourth-order homogeneous ordinary differential equations have the general solutions

$$\begin{aligned}\mathcal{S}_{S/B} = {} & [C_1^{S/B}\cos(\zeta_{S/B}^-) + C_2^{S/B}\sin(\zeta_{S/B}^-)]e^{-\zeta_{S/B}^+} \\ & + [C_3^{S/B}\cos(\zeta_{S/B}^-) + C_4^{S/B}\sin(\zeta_{S/B}^-)]e^{\zeta_{S/B}^+},\end{aligned}$$

where $C_{1,2,3,4}^{S/B}$ are constant determined by the boundary conditions and $\zeta_{S/B}^{\pm}$ are stretched surface and bottom boundary layer vertical coordinates defined as $\zeta_S^{\pm} = z/\delta_{\pm}$ and $\zeta_B^{\pm} = (z+H)/\delta_{\pm}$, respectively, with the typical length scales $\delta_{\pm} = \sqrt{2\nu/(\sqrt{f^2+\lambda^2} \pm \lambda)}$.

First, we focus on the surface boundary equation. To determine the constants, we impose the solution $\mathcal{S}_S$ to gently merge to the interior solution for $z \ll -\delta_+$ (or $\zeta_S^+ \to -\infty$), so that $C_1^S = C_2^S = 0$. Then we apply the surface boundary conditions at the surface ($z = 0$), linked to the wind stress: $\nu\partial_z\overline{u}|_0 = \overline{\tau}_x/\rho_0$ and $\nu\partial_z\overline{v}|_0 = \overline{\tau}_y/\rho_0$. These two conditions could be expressed as

$$\mathcal{S}|_0 = -\frac{W}{\rho_0\nu}\overline{\tau}_y, \quad \text{and} \quad \text{(B5a)}$$

$$\partial_z^2\mathcal{S}|_0 = \frac{gW}{\rho_0\nu}\partial_y\overline{\rho}|_0 - \frac{W}{\rho_0\nu^2}(f\overline{\tau}_x + \lambda\overline{\tau}_y). \quad \text{(B5b)}$$

They determine the two remaining constants as

$$C_3^S = -\frac{W}{\rho_0\nu}\overline{\tau}_y - \mathcal{S}_I|_0, \quad \text{(B6a)}$$

$$\begin{aligned}C_4^S = {} & \frac{\delta_+\delta_-}{2}\left[\left(\frac{1}{\delta_-^2} - \frac{1}{\delta_+^2}\right)C_3^S \right. \\ & \left. + \frac{gW}{\rho_0\nu}\partial_y\overline{\rho}|_0 - \partial_z^2\mathcal{S}_I|_0 - \frac{W}{\rho_0\nu^2}(f\tau_x + \lambda\tau_y)\right]. \quad \text{(B6b)}\end{aligned}$$

Thus, the shear for the surface boundary layer correction is

$$\begin{aligned}\mathcal{S}_S = e^{z/\delta_+}\left\{ {} & -\left(\frac{W}{\rho_0\nu}\overline{\tau}_y + \mathcal{S}_I|_0\right)\cos\left(\frac{z}{\delta_-}\right) \right. \\ & + \frac{\delta_+\delta_-}{2}\left[\left(\frac{1}{\delta_+^2} - \frac{1}{\delta_-^2}\right)\left(\frac{W}{\rho_0\nu}\overline{\tau}_y + \mathcal{S}_I|_0\right)\right. \\ & \left.\left. + \frac{gW}{\rho_0\nu}\partial_y\overline{\rho}|_0 - \partial_z^2\mathcal{S}_I|_0 - \frac{W}{\rho_0\nu^2}(f\tau_x + \lambda\tau_y)\right]\sin\left(\frac{z}{\delta_-}\right)\right\}. \quad \text{(B7)}\end{aligned}$$

Following the same methodology for the bottom boundary layer, we obtain $C_3^B = C_4^B = 0$ so that the solution gently merges to the interior solution (when $\zeta_B^+ \to +\infty$). We also apply a free-slip boundary condition at the bottom ($\partial_z\overline{u}|_{-H} = \partial_z\overline{v}|_{-H} = 0$). These conditions could be expressed as

$$\mathcal{S}|_{-H} = 0, \quad \text{and} \quad \text{(B8a)}$$

$$\partial_z^2\mathcal{S}|_{-H} = \frac{gW}{\rho_0\nu}\partial_y\overline{\rho}|_{-H}. \quad \text{(B8b)}$$

These conditions lead to

$$C_1^B = -\mathcal{S}_I|_{-H}, \quad \text{and} \quad \text{(B9a)}$$

$$C_2^B = \frac{\delta_+\delta_-}{2}\left[\left(\frac{1}{\delta_+^2} - \frac{1}{\delta_-^2}\right)C_1^B - \frac{gW}{\rho_0\nu}\partial_y\overline{\rho}|_{-H} + \partial_z^2\mathcal{S}_I|_{-H}\right]. \quad \text{(B9b)}$$

We obtain the shear correction for the bottom boundary as

$$\begin{aligned}\mathcal{S}_S = e^{-(z+H)/\delta_+}\left\{ {} & -\mathcal{S}_I|_{-H}\cos\left(\frac{z+H}{\delta_-}\right) \right. \\ & + \frac{2}{\delta_+\delta_-}\left[\left(\frac{1}{\delta_-^2} - \frac{1}{\delta_+^2}\right)\mathcal{S}_I|_{-H}\right. \\ & \left.\left. - \frac{gW}{\rho_0\nu}\partial_y\overline{\rho}|_{-H} + \partial_z^2\mathcal{S}_I|_{-H}\right]\sin\left(\frac{z+H}{\delta_-}\right)\right\}. \quad \text{(B10)}\end{aligned}$$

By using these expressions and $\mathcal{S} = \mathcal{S}_I + \mathcal{S}_S + \mathcal{S}_B$, we have a general expression for the vertical shear of the zonally averaged meridional velocity.

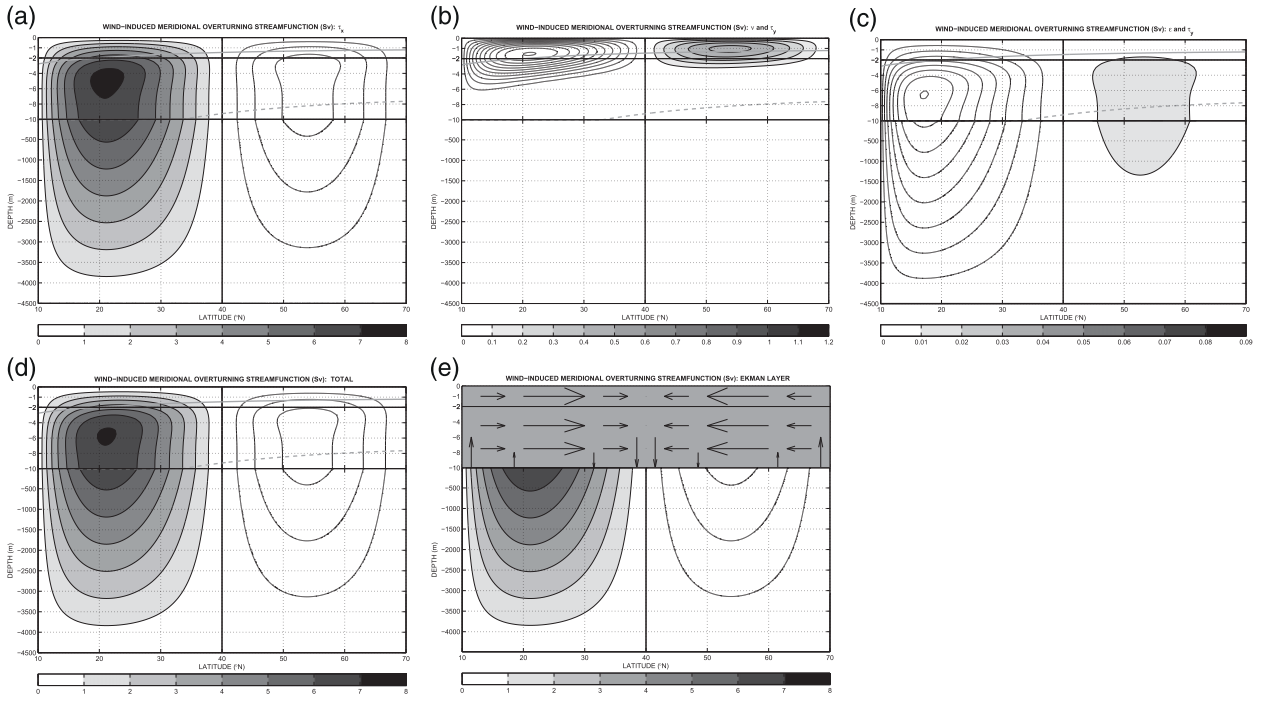

FIG. B1. (a)–(c) The three terms of the wind-induced AMOC for the explicit vertical boundary case. Circulation induced by (a) the zonal wind stress, (b) the meridional wind stress together with vertical viscosity, and (c) the meridional wind stress together with Rayleigh friction. Note the scale separation between the three circulations. (d) The sum of (a),(b), and (c). (e) The solution when a surface Ekman boundary is imposed in the first 10 m of the ocean, that is, the implicit surface boundary case. The vertical axis is not linear. Grayscale shading is superimposed to the contours for positive values (following the white-to-black color bar scale). Negative values are shown by contours without the white-to-black shading superimposed. Positive values denote clockwise circulation, and (a)–(d) the solid and dashed gray lines correspond to the two typical length scales of the surface boundary layer: the e-folding decay length scale δ_+ and the wavelength $2\pi\delta_-$. The gray area in (e) represents the Ekman layer, where the arrows show the direction and the intensity of the flow. Below a depth corresponding to the wavelength of the surface boundary layer ($2\pi\delta_- \simeq 10$ m) the two cases, (d) and (e), are almost identical.

3) THE TOTAL SOLUTION

By using $\partial_z^2\psi = \mathcal{S}$ and the two remaining boundary conditions (i.e., $\overline{w}|_{-H} = \overline{w}|_0 = 0$, these terms being equivalent to $\psi|_{-H} = \psi|_0 = 0$), we are able to determine the total flow. The general solutions of the vertical velocity and of the streamfunction are

$$\partial_z\psi = -W\overline{v} = A + \frac{1}{(f^2+\lambda^2)\rho_0}[\lambda W\partial_y\overline{P} - f(P|_{x_E} - P|_{x_W})] + \mathcal{P}_1(\mathcal{S}_S) + \mathcal{P}_1(\mathcal{S}_B), \quad \text{and} \tag{B11}$$

$$\psi = Az + B + \frac{1}{(f^2+\lambda^2)\rho_0}\int_z^0 [f(P|_{x_E} - P|_{x_W}) - \lambda W\partial_y\overline{P}]\,dz + \mathcal{P}_2(\mathcal{S}_S) + \mathcal{P}_2(\mathcal{S}_B), \tag{B12}$$

where A and B are two unknowns, the first z primitive of the surface and bottom shear are

$$\mathcal{P}_1(\mathcal{S}_S) = \frac{\delta_+\delta_-}{\delta_+^2+\delta_-^2}\left[(\delta_- C_3^S - \delta_+ C_4^S)\cos\left(\frac{z}{\delta_-}\right) + (\delta_+ C_3^S + \delta_- C_4^S)\sin\left(\frac{z}{\delta_-}\right)\right]e^{z/\delta_+}, \quad \text{and} \tag{B13a}$$

$$\mathcal{P}_1(\mathcal{S}_B) = -\frac{\delta_+\delta_-}{\delta_+^2+\delta_-^2}\left[(\delta_- C_1^B + \delta_+ C_2^B)\cos\left(\frac{z+H}{\delta_-}\right) + (\delta_- C_2^B - \delta_+ C_1^B)\sin\left(\frac{z+H}{\delta_-}\right)\right]e^{-(z+H)/\delta_+}, \tag{B13b}$$

and the second z primitive is

$$\mathcal{P}_2(\mathcal{S}_S) = \left(\frac{\delta_+\delta_-}{\delta_+^2+\delta_-^2}\right)^2\left\{[(\delta_-^2-\delta_+^2)C_3^S - 2\delta_+\delta_- C_4^S]\cos\left(\frac{z}{\delta_-}\right) + [2\delta_+\delta_- C_3^S + (\delta_-^2-\delta_+^2)C_4^S]\sin\left(\frac{z}{\delta_-}\right)\right\}e^{z/\delta_+}, \quad \text{and} \tag{B14a}$$

$$\mathcal{P}_2(\mathcal{S}_B)=\left(\frac{\delta_+\delta_-}{\delta_+^2+\delta_-^2}\right)^2\left\{[(\delta_-^2-\delta_+^2)C_1^B+2\delta_+\delta_-C_2^B]\cos\left(\frac{z+H}{\delta_-}\right)+[-2\delta_+\delta_-C_1^B+(\delta_-^2-\delta_+^2)C_2^B]\sin\left(\frac{z+H}{\delta_-}\right)\right\}e^{-(z+H)/\delta_+}. \tag{B14b}$$

Applying the boundary conditions we obtain the two last unknowns:

$$\psi|_0=0 \quad\Leftrightarrow\quad B=\left(\frac{\delta_+\delta_-}{\delta_+^2+\delta_-^2}\right)^2[2\delta_+\delta_-C_4^S-(\delta_-^2-\delta_+^2)C_3^S], \quad \text{and} \tag{B15a}$$

$$\psi|_{-H}=0 \quad\Leftrightarrow\quad A=\frac{1}{(f^2+\lambda^2)\rho_0}[f(\langle P\rangle|_{x_E}-\langle P\rangle|_{x_W})-\lambda W\partial_y\langle\overline{P}\rangle]+\frac{1}{H}\left(\frac{\delta_+\delta_-}{\delta_+^2+\delta_-^2}\right)^2[(\delta_-^2-\delta_+^2)(C_1^B-C_3^S)+2\delta_+\delta_-(C_2^B+C_4^S)]. \tag{B15b}$$

Thus, for the explicit boundary layers, the analytical expressions of the solution are straightforward, despite the expression being quite intricate. However, to keep the manuscript as readable as possible, and given that both explicit and implicit cases only show minor differences (validating the use of the Ekman layer), we have not expressed the full solution for the explicit surface boundary layers. A more extensive discussion on the wind-induced circulation in the surface boundary layer and its relation to Ekman layer is done next.

b. *Wind-induced circulation: Implicit versus explicit vertical boundary layers*

Unlike the thermohaline part of the AMOC, the wind-induced part can be exactly obtained without any approximation on the unidirectionality of the horizontal flow. The wind-induced circulation is directly affected by our choice of implicit or explicit vertical boundary layers. In the former case, the interior solution (below the surface boundary layer set to 10 m) is patched to a surface Ekman layer. The resulting circulation is thus only affected by the zonally averaged zonal wind stress (Fig. B1). In the latter case, the solution can be decomposed in three terms: (i) one due to the zonally averaged zonal wind stress (Fig. B1a), (ii) one due to the zonally averaged meridional wind stress through the vertical viscosity (Fig. B1b), and (iii) one due to the zonally averaged meridional wind stress through the linear Rayleigh friction (Fig. B1c). The sum of these three terms gives the total wind-induced circulation (Fig. B1d).

The three terms of wind-induced circulation for the explicit boundary layers case are almost separated by an order of magnitude: (i) peaking at several Sverdrup, (ii) at a Sverdrup, and (iii) at a deci-Sverdrup. Their spatial scale is also different, whereas terms i and iii reach the bottom, term ii is confined in the first meters of the ocean. Both wind-induced circulations due to the zonally averaged meridional wind stress reduce the effect of the zonally averaged zonal wind stress (Figs. B1b,c vs Fig. B1a). Note that on a much wider basin such as the Pacific (i.e., up to 5 times as wide as the Atlantic), the effect of zonally averaged meridional wind stress through the vertical viscosity could reach 6 Sv but would still be localized in a thin layer of the upper ocean.

The comparison between the explicit and implicit boundary layers cases hardly shows any difference below 10 m (Fig. B1d vs Fig. B1e). This acknowledges the validity of the Ekman surface layer to properly treat the surface boundary layer and to propagate the ocean surface boundary conditions (the wind stresses) to the interior solution. This comparison also suggests that the interior solution is valid below a depth equal to the Ekman wavelength, that is, the Ekman boundary layer thickness is well parameterized using the Ekman wavelength: $2\pi\delta_- \simeq 2\pi\sqrt{2\nu/f} \simeq 10$ m (the dashed gray line in Figs. B1a–d) rather than using the e-folding decay length scale: $\delta_+ \simeq \sqrt{2\nu/f}$ (the solid gray line in Figs. B1a–d).

REFERENCES

Barreiro, M., A. Fedorov, R. Pacanowski, and S. G. Philander, 2008: Abrupt climate changes: How freshening of the northern Atlantic affects the thermohaline and wind-driven oceanic circulations. *Rev. Earth Planet. Sci.*, **36**, 33–58, doi:10.1146/annurev.earth.36.090507.143219.

Boussinesq, J., 1903: *Théorie Analytique de la Chaleur.* Vol. 2. Gautier-Villars, 625 pp.

Broecker, W. S., G. Bond, M. Klas, G. Bonani, and W. Wolfli, 1990: A salt oscillator in the glacial Atlantic? 1. The concept. *Paleoceanography*, **5**, 469–477, doi:10.1029/PA005i004p00469.

Bryden, H. L., 1976: Horizontal advection of temperature for low-frequency motions. *Deep-Sea Res. Oceanogr. Abstr.*, **23**, 1165–1174, doi:10.1016/0011-7471(76)90892-5.

——, 1980: Geostrophic vorticity balance in midocean. *J. Geophys. Res.*, **85**, 2825–2828, doi:10.1029/JC085iC05p02825.

Colin de Verdière, A., 1988: Buoyancy driven planetary flow. *J. Mar. Res.*, **46**, 215–265, doi:10.1357/002224088785113667.

——, and R. Tailleux, 2005: The interaction of a baroclinic mean flow with long Rossby waves. *J. Phys. Oceanogr.*, **35**, 865–879, doi:10.1175/JPO2712.1.

——, and L. te Raa, 2010: Weak oceanic heat transport as a cause of the instability of glacial climates. *Climate Dyn.*, **35**, 1237–1256, doi:10.1007/s00382-009-0675-8.

——, M. Ben Jelloul, and F. Sévellec, 2006: Bifurcation structure of thermohaline millennial oscillation. *J. Climate*, **19**, 5777–5795, doi:10.1175/JCLI3950.1.

Cunningham, S., and Coauthors, 2007: Temporal variability of the Atlantic meridional overturning circulation at 26.5°N. *Science*, **317**, 935–937, doi:10.1126/science.1141304.

de Boer, A. M., A. Gnanadesikan, N. R. Edwards, and A. J. Watson, 2010: Meridional density gradients do not control the Atlantic overturning circulation. *J. Phys. Oceanogr.*, **40**, 368–380, doi:10.1175/2009JPO4200.1.

Drbohlav, J., and F. F. Jin, 1998: Interdecadal variability in a zonally averaged ocean model: An adjustment oscillator. *J. Phys. Oceanogr.*, **28**, 1252–1270, doi:10.1175/1520-0485(1998)028<1252:IVIAZA>2.0.CO;2.

Ferreira, D., J. Marshall, and J.-M. Campin, 2010: Localization of deep water formation: Role of atmospheric moisture transport and geometrical constraints on ocean circulation. *J. Climate*, **23**, 1456–1476, doi:10.1175/2009JCLI3197.1.

Gagosian, R. B., 2003: Abrupt climate change: Should we be worried? *World Economic Forum*, Davos, Switzerland, Woods Hole Oceanographic Institution. [Available online at http://www.whoi.edu/page.do?pid=83339&tid=3622&cid=9986.]

Ganachaud, A., and C. Wunsch, 2000: Improved estimates of global ocean circulation, heat transport and mixing from hydrographic data. *Nature*, **408**, 453–457, doi:10.1038/35044048.

Giarolla, E., P. Nobre, M. Malagutti, and L. P. Pezzi, 2005: The Atlantic Equatorial Undercurrent: PIRATA observations and simulations with GFDL Modular Ocean Model at CPTEC. *Geophys. Res. Lett.*, **32**, L10617, doi:10.1029/2004GL022206.

Gnanadesikan, A., 1999: A simple predictive model for the structure of the oceanic pycnocline. *Science*, **283**, 2077–2079, doi:10.1126/science.283.5410.2077.

Haertel, P., and A. V. Fedorov, 2012: The ventilated ocean. *J. Phys. Oceanogr.*, **42**, 141–164, doi:10.1175/2011JPO4590.1.

Hirschi, J., and J. Marotzke, 2007: Reconstructing the meridional overturning circulation from boundary densities and the zonal wind stress. *J. Phys. Oceanogr.*, **37**, 743–763, doi:10.1175/JPO3019.1.

——, J. Baehr, J. Marotzke, J. Stark, S. Cunningham, and J.-O. Beismann, 2003: A monitoring design for the Atlantic meridional overturning circulation. *Geophys. Res. Lett.*, **30**, 1413, doi:10.1029/2002GL016776.

Howard, L. N., 1971: ABC's of convection. Geophysical Fluid Dynamics Summer School. WHOI Internal Tech. Rep. 71-63, 102–105.

Huang, R. X., 2010: *Ocean Circulation, Wind-Driven and Thermohaline Processes*. Cambridge University Press, 791 pp.

——, and W. Wang, 2003: Gravitational potential energy sinks/sources in the oceans. *Near-Boundary Processes and Their Parameterization: Proc. 'Aha Huliko'a Hawaiian Winter Workshop*, Honolulu, HI, University of Hawai'i at Mānoa, 239–247.

Huck, T., A. J. Weaver, and A. Colin de Verdiére, 1999: On the influence of the parameterization of lateral boundary layers on the thermohaline circulation in coarse-resolution ocean models. *J. Mar. Res.*, **57**, 387–426, doi:10.1357/002224099764805138.

Johnson, H. L., and D. P. Marshall, 2002: A theory for the surface Atlantic response to thermohaline variability. *J. Phys. Oceanogr.*, **32**, 1121–1132, doi:10.1175/1520-0485(2002)032<1121:ATFTSA>2.0.CO;2.

Killworth, P. D., 1992: An equivalent-barotropic mode in the fine resolution Antarctic model. *J. Phys. Oceanogr.*, **22**, 1379–1387, doi:10.1175/1520-0485(1992)022<1379:AEBMIT>2.0.CO;2.

——, and C. W. Hughes, 2002: The Antarctic Circumpolar Current as a free equivalent-barotropic jet. *J. Mar. Res.*, **60**, 19–45, doi:10.1357/002224002762341230.

Knutti, R., T. F. Stocker, and D. G. Wright, 2000: The effects of subgrid-scale parameterizations in a zonally averaged ocean model. *J. Phys. Oceanogr.*, **30**, 2738–2752, doi:10.1175/1520-0485(2000)030<2738:TEOSSP>2.0.CO;2.

Koltermann, K. P., V. V. Gouretski, and K. Jancke, 2011: *Atlantic Ocean*. Vol. 3, *Hydrographic Atlas of the World Ocean Circulation Experiment (WOCE)*, M. Sparrow, P. Chapman, and J. Gould, Eds., International WOCE Project Office, 174 pp.

Lumpkin, R., and K. Speer, 2007: Global ocean meridional overturning. *J. Phys. Oceanogr.*, **37**, 2550–2562, doi:10.1175/JPO3130.1.

Madec, G., P. Delecluse, M. Imbard, and C. Lévy, 1998: OPA 8.1 ocean general circulation model reference manual. L'Institut Pierre-Simon Laplace Tech. Rep. 11, 91 pp.

Malkus, W. V. R., 1972: Non-periodic convection at high and low Prandtl number. *Mém. Soc. Roy. Sci. Liége*, **4**, 125–128.

Manabe, S., and R. J. Stouffer, 1995: Simulation of abrupt climate change induced by freshwater input by freshwater input to the North Atlantic. *Nature*, **378**, 165–167, doi:10.1038/378165a0.

——, and ——, 1999: The role of thermohaline circulation in climate. *Tellus*, **51A**, 91–109, doi:10.1034/j.1600-0889.1999.00008.x.

Marotzke, J., P. Welander, and J. Willebrand, 1988: Instability and multiple steady states in a meridional-plane model of the thermohaline circulation. *Tellus*, **40A**, 162–172, doi:10.1111/j.1600-0870.1988.tb00414.x.

McCarthy, G., and Coauthors, 2012: Observed interannual variability of the Atlantic meridional overturning circulation at 26.5°N. *Geophys. Res. Lett.*, **39**, L19609, doi:10.1029/2012GL052933.

Munk, W. H., 1950: On the wind-driven ocean circulation. *J. Meteor.*, **7**, 80–93, doi:10.1175/1520-0469(1950)007<0080:OTWDOC>2.0.CO;2.

Nikurashin, M., and G. Vallis, 2012: A theory of the interhemispheric meridional overturning circulation and associated stratification. *J. Phys. Oceanogr.*, **42**, 1652–1667, doi:10.1175/JPO-D-11-0189.1.

Olbers, D., J. Willebrand, and C. Eden, 2012: *Ocean Dynamics*. Springer-Verlag, 708 pp.

Park, Y.-G., and K. Bryan, 2000: Comparison of thermally driven circulations from a depth-coordinate model and an isopycnal-layer model. Part I: Scaling-law sensitivity to vertical diffusivity. *J. Phys. Oceanogr.*, **30**, 590–605, doi:10.1175/1520-0485(2000)030<0590:COTDCF>2.0.CO;2.

Pedlosky, J., 1979: *Geophysical Fluid Dynamics*. Springer-Verlag, 626 pp.

Phillips, N. A., 1963: Geostrophic motions. *Rev. Geophys.*, **1**, 123–176, doi:10.1029/RG001i002p00123.

Rahmstorf, S., 1995: Bifurcation of the Atlantic thermohaline circulation in response to changes in the hydrological cycle. *Nature*, **378**, 145–149, doi:10.1038/378145a0.

Rayner, D., and Coauthors, 2011: Monitoring the Atlantic meridional overturning circulation. *Deep-Sea Res.*, **12**, 1744–1753, doi:10.1016/j.dsr2.2010.10.056.

Rind, D., P. deMenocal, G. Russell, S. Sheth, D. Collins, G. Schmidt, and J. Teller, 2001: Effect of glacial meltwater in GISS coupled atmosphere-ocean model: 1. North Atlantic Deep Water response. *J. Geophys. Res.*, **106**, 27 335–27 353, doi:10.1029/2000JD000070.

Salmon, R., 1998: *Lectures on Geophysical Fluid Dynamics.* Oxford University Press, 400 pp.

Sandström, J. W., 1908: Dynamische Versuche mit Meerwasser. *Ann. Hydrogr. Marit. Meteor.*, **36**, 6–23.

Schott, F., and H. Stommel, 1978: Beta spirals and absolute velocities in different oceans. *Deep-Sea Res.*, **25**, 961–1010, doi:10.1016/0146-6291(78)90583-0.

Sévellec, F., and A. V. Fedorov, 2011: Stability of the Atlantic meridional overturning circulation in a zonally-averaged ocean model: The effects of freshwater flux, wind stress, and diapycnal diffusion. *Deep-Sea Res. II*, **58**, 1927–1943, doi:10.1016/j.dsr2.2010.10.070.

——, T. Huck, and M. Ben Jelloul, 2006: On the mechanism of centennial thermohaline oscillations. *J. Mar. Res.*, **64**, 355–392, doi:10.1357/002224006778189608.

——, ——, and A. Colin de Verdière, 2010: From centennial to millennial oscillation of the thermohaline circulation. *J. Mar. Res.*, **68**, 723–742, doi:10.1357/002224011795977635.

Sijp, W. P., J. M. Gregory, R. Tailleux, and P. Spence, 2012: The key role of the western boundary in linking the AMOC strength to the north–south pressure gradient. *J. Phys. Oceanogr.*, **42**, 628–643, doi:10.1175/JPO-D-11-0113.1.

Spall, M. A., 1992: Cooling spirals and recirculation in the Subtropical Gyre. *J. Phys. Oceanogr.*, **22**, 564–571, doi:10.1175/1520-0485(1992)022<0564:CSARIT>2.0.CO;2.

Spiegel, E. A., and G. Veronis, 1960: Boussinesq approximation for a compressible fluid. *Astrophys. J.*, **131**, 442–447, doi:10.1086/146849.

Stocker, T. F., L. A. Mysak, and D. G. Wright, 1992: A zonally averaged, coupled ocean–atmosphere model for paleoclimate studies. *J. Climate*, **5**, 773–797, doi:10.1175/1520-0442(1992)005<0773:AZACOA>2.0.CO;2.

Stommel, H., 1948: The westward intensification of wind-driven ocean currents. *Eos, Trans. Amer. Geophys. Union*, **29**, 202–206, doi:10.1029/TR029i002p00202.

——, 1958: The abyssal circulation. *Deep-Sea Res.*, **5**, 80–82, doi:10.1016/S0146-6291(58)80014-4.

——, 1961: Thermohaline convection with stable regimes flow. *Tellus*, **13A**, 224–230, doi:10.1111/j.2153-3490.1961.tb00079.x.

——, and A. B. Arons, 1960a: On the abyssal circulation of the World Ocean—I. Stationary planetary flow patterns on a sphere. *Deep-Sea Res.*, **6**, 140–154, doi:10.1016/0146-6313(59)90065-6.

——, and ——, 1960b: On the abyssal circulation of the World Ocean—II. An idealized model of the circulation pattern and amplitude in oceanic basins. *Deep-Sea Res.*, **6**, 217–233, doi:10.1016/0146-6313(59)90075-9.

Stouffer, R. J., and Coauthors, 2006: Investigating the causes of the response of the thermohaline circulation to past and future climate changes. *J. Climate*, **19**, 1365–1387, doi:10.1175/JCLI3689.1.

Sverdrup, H. U., 1947: Wind-driven currents in a baroclinic ocean; with application to the equatorial current of eastern Pacific. *Proc. Natl. Acad. Sci. USA*, **33**, 318–326, doi:10.1073/pnas.33.11.318.

Talley, L. D., J. L. Reid, and P. E. Robbins, 2003: Data-based meridional overturning streamfunctions for the global ocean. *J. Climate*, **16**, 3213–3226, doi:10.1175/1520-0442(2003)016<3213:DMOSFT>2.0.CO;2.

Vallis, G. K., 2006: *Atmospheric and Oceanic Fluid Dynamics.* Cambridge University Press, 769 pp.

Vellinga, M., and R. A. Wood, 2002: Global climatic impacts of a collapse of the Atlantic thermohaline circulation. *Climatic Change*, **54**, 251–267, doi:10.1023/A:1016168827653.

Wolfe, C. L., and P. Cessi, 2011: The adiabatic pole-to-pole overturning circulation. *J. Phys. Oceanogr.*, **41**, 1795–1810, doi:10.1175/2011JPO4570.1.

Wright, D. G., and T. F. Stocker, 1991: A zonally averaged ocean model for thermohaline circulation. Part I: Model development and flow dynamics. *J. Phys. Oceanogr.*, **21**, 1713–1724, doi:10.1175/1520-0485(1991)021<1713:AZAOMF>2.0.CO;2.

——, and ——, 1992: Sensitivities of a zonally averaged global ocean circulation model. *J. Geophys. Res.*, **97**, 12 707–12 730, doi:10.1029/92JC01168.

——, C. B. Vreugdenhil, and T. M. Hughes, 1995: Vorticity dynamics and zonally averaged ocean circulation models. *J. Phys. Oceanogr.*, **25**, 2141–2154, doi:10.1175/1520-0485(1995)025<2141:VDAZAO>2.0.CO;2.

——, T. F. Stocker, and D. Mercer, 1998: Closures used in zonally averaged ocean models. *J. Phys. Oceanogr.*, **28**, 791–804, doi:10.1175/1520-0485(1998)028<0791:CUIZAO>2.0.CO;2.